UNIVERSITAT POLITÈCNICA DE VALÈNCIA

School of Aerospace Engineering and Industrial Design

Parametric study of the effect of the efficiencies of an ejectors model over its capabilities

End of Degree Project

Bachelor's Degree in Aerospace Engineering

AUTHOR: Ianosel Macavei, Nicola María

Tutor: Dolz Ruiz, Vicente

ACADEMIC YEAR: 2023/2024

Parametric study of the effect of the different values of the efficiencies of an ejector's model over its capabilities.

Universitat Politècnica de València

Escuela Técnica Superior de Ingeniería del Diseño

Degree: Aerospace Engineering

Author:

Nicola Maria Ianosel Macavei

Project tutor:

Vicente Dolz Ruiz

June 12, 2024

Abstract

The goal of this final degree project is the parametric study of the efficiencies of the Simescape model of an ejector, which is an element that is used to compress a gas that has low pressure (secondary flow) by taking advantage of the expansion of another gas which has high pressure (primary flow). The primary flow is expanded, which sucks in the secondary flow, which gives as a result a mixture of flows that is found at intermediate pressure. This element is very used in ejection cycles, which allows the refrigeration of systems by using and taking advantage of the residual heat from the same. They are also used in purge circuits or in lubricant oil recovery and in gas recirculation in hydrogen fuel cells. The aforementioned model functions properly when the working fluid inside of it is found fully in gas phase. However, when working close to the saturated vapor conditions, phenomena of local condensation in the expansion processes can occur, which compromise the accuracy of the model. To study this piece, a perfect, semi perfect and real models of the gas are going to be used to simulate diverse operational conditions, by fixing the outlet pressure and varying the inlet pressure of the secondary and primary flows, and using these data to generate the working map of the ejector. This procedure is going to be repeated for while altering the 4 different efficiencies that govern the operation of the piece, which the ultimate goal of determining in what ranges does the piece work correctly, but also to evaluate how choosing a certain value of an efficiency affects the outcome of the results.

Keywords: parametric study; ejector; simescape; matlab; efficiencies; perfect gas; semi-perfect gas; real gas; operating map;

Contents

Nomenclature

Symbols	Definition	Magnitude
ω	Ejector entrainment ratio	[-]
p	Pressure	[MPA]
h	Specific enthalpy	$\left[\frac{kJ}{kg}\right]$
s	Specific entropy	$\left[\frac{kJ}{kg \cdot K}\right]$
M	Mass Flow	$\left[\frac{kg}{s}\right]$
X	Vapor Quality	[-]
T	Temperature	[K]
p_P	Primary flow pressure	[Pa]
p_S	Secondary flow pressure	[Pa]
p_{outlet}	Outlet pressure	[Pa]
p_O	Operating pressure	[Pa]
$\dot{m}_P$	Primary flow mass flow	$\left[\frac{kg}{s}\right]$
$\dot{m}_S$	Secondary flow mass flow	$\left[\frac{kg}{s}\right]$

Glossary

CAD Computer-Aided Design. 15

CMT Centro de Motores Térmicos. 3

M Mixing. 43, 54

PE Primary Flow Expansion. 42, 54

PN Primary flow through nozzle. 40, 54

SDG Sustainable Development Goals. 60, 61, 85

SS Secondary flow suction. 39, 53

1 Introduction

1.1 Project background and emergence

The rapid development in computational science has allowed for the creation of better, faster, more accurate and reliable programs that enable engineers and scientists of all disciplines to test and model the processes, items or materials that will later be constructed. This has an advantage regarding resource and time management, since its is less time consuming to model a system than to build it, as well as having a reduced cost. Moreover, in case of failure, there is no resources waste, because the model can be adapted until the desired output is obtained and then build the ultimate and perfected version.

One of these modelling tools is Simulink, a graphical environment based on the programming language Matlab and, within which, the Simscape library is found. This is a library that is specifically designed for the modelling of physical systems such as electrical, hydraulic or refrigeration systems, as well as providing the necessary tools for data acquisition and analysis. This modelling environment is has many advantages, the main one being that it is very visual, which allows for an easy implementation and design, as well as understanding of the model.

Using Simscape is a very profitable way of performing analysis of cycles such as can be a refrigeration cycle, and it is no wonder that the CMT, which is a research and development institution found within the *Universitat Politènica de Valencia*, chose this software when the task of modelling an ejection cycle was entrusted to them.

An ejection cycle is a type of refrigeration cycle that uses an ejector to recover heat from a high temperature source and uses this energy to further cool down a system. There are mathematical models of the ejector piece in the Simescape library, but it presents some limitations, such as:

- All of the fluids that go across it must be in gas state in their totality.

- The fluid inside the nozzle is considered isentropic, with efficiencies, and it only models (if necessary) 1 normal shockwave in the mixing channel. When operating in reverse flow conditions, there may be more shock waves formed, which are not modelled, and this can lead in inaccuracies in the results

When the CMT started parametrizing the cycle at study, they found that the refrigerant around which the tests were to be performed, the R1234yf, entered the ejector in gas state but after the mixing process inside it, it came out gas with some condensation droplets, and this is something that the simulation cannot sustain. Note that the problem was not due to the usage of this refrigerant type, but rather of the programming of the simescape model, which cannot sustain phase change within it. This led to errors and limitations in the modelling process, since

the amount of assumptions and simplifications that were required in order to avoid these errors made the model too different from the real system at study. This has as a consequence that the results obtained from these tests cannot be used or extrapolated to the real life situation, or can be utilized in a very small percentage.

Thus, this present project emerged, as a research paper for the development of the working map that the Simscape model of an ejector piece has. Additionally, different states of the chosen working fluid, the R1234yf, have been analysed, for a broader and more realistic application of the conclusions found in this paper. Furthermore, this project also aims to qualitatively asses how the model operates when dealing with reverse flow, seeing how it differs between the real case and the simplified one.

1.2   Goals

This paper has emerged with two objectives in mind. The first one is observing and analysing the results that the simplified model gives when dealing with reserve flow, which is something that it is not modelled for, and see how much the accuracy of the same is affected by this limitation.

In order to do this, the development of the working maps of the piece are generated. These are three-dimensional graphics that relate the three most representative parameters that define the operation of an ejector, and that will later be thoroughly explained: entrainment ratio and pressure ratios. By observing these three variables, the different operating domains can be observed and quantified.

Additionally, this paper also aims to perform a sensitivity analysis of the model upon different values of the efficiencies that define the piece of the ejector, by varying their value within a certain range and comparing it with the chosen base case, and see how much the choice of one value or other affects the final result.

In order to simplify the analysis, there will be chosen some values of the primary pressure ratios and they will be plotted in a graph against the secondary pressure ratio and entrainment ratio.

For a broader application, these maps will be developed not only for the ideal gas state of the refrigerant of choice, the R1234yf, but also the perfect gas and real gas states. In subsequent sections, all the physical characteristics and assumptions made regarding each of these states of the refrigerant will be detailed.

With these results, a more profound and complete understanding of the working limitations of the model can be attained, which can in turn lead to a better screening process of what cycles have the potential of being decently modelled using this piece.

1.3   Methodology followed and structure of the document

To achieve the goals presented in the previous section, a thorough method should be employed, so that time is efficiently utilised and resources are not wasted or misused. The steps followed also coincide to some degree with the way this document has been divided, and will now be itemized.

To begin with, a theoretical background, in Section 2, with the explanation of the physical phenomena and laws that dominate the ejector is found, so that the reader can have all the necessary information and data required for the understanding of the process studied. Some of the concepts explained range from the definition of what a refrigeration cycle is, the difference between an ideal, perfect and real gas or the thermodynamic cycles that represent the physical transformations within an ejector.

Next, in Section 3, an explanation of the Simscape model employed to run the different simulations is found, with thorough detailing of all the different variables and parameters that are set for the diverse elements. In this section, a description of the three different models of the working fluids at use is performed.

With the data from the simulations, in Section 4, a database is build, so that the three-dimensional graphs that represent the working map of the ejectors, as well as the two-dimensional plots for certain primary pressure ratios can be generated and compared. These are going to be analysed and compared so that, in the following section, Section 5, a summary of all the conclusions obtained will be written.

Last but not least, the Appendix A will be found, where the scopes statement of this project can be found together with a breakdown of the costs that the development of this project has. The scopes statement is a document that details a projects main objectives wit their corresponding criteria for success measurement. In the appendix it can also be found the different data tables obtained and generated during the project, but that are not crucial for the understanding of the same.

2 Theoretical background

For the reader to properly comprehend all the ideas that compose this project, this section is redacted. Its aim is to explain the fundamental theoretical concepts upon which the research is performed, ensuring that the conclusions obtained are fully understood.

Even though this research revolves around the ejector, it is important to understand how it works within the basic ejection refrigeration cycle, which has an p-h diagram associated. This is a diagram that relates the specific enthalpy (h) to the pressure (p), and indicates the different physical states in which a fluid can be found, and that are going to be described in a few pages. Last but not least, considering that the refrigerant at study will be analysed as an ideal, perfect and real gas, the characteristics and main differences of all of these will be detailed, and how utilising one or another one alters the p-h diagram of the cycle.

2.1 Physical and thermodynamic properties

A physical property is any measurable quality involved in a physical system and gives information about an object's state or behaviour. The variation of these is what gives information about the changes that take an object or process from one state to the other. They can be intensive properties, if they do not depend on the amount of matter, such as density, or extensive, which do depend on the amount of matter, such can be the case of mass or volume.

The most important ones for the sake of understanding this paper are the pressure and the temperature, both of them intensive properties.

Pressure is defined as the ratio between the force applied perpendicularly over an object and the area of application. For this paper, it is necessary to understand what back pressure is: it is the pressure of a fluid that is used to define the resistance to flow through a system due to the generation of friction or any other source of obstacle.

Temperature it reflects the average kinetic energy of the vibrating atoms that make up a substance.

Thermodynamic properties are characteristic features of a system that are capable of specifying its state. For this paper, the most used thermodynamic property if the enthalpy, or more precisely, the specific enthalpy, which is the enthalpy per unit mass. Enthalpy is the sum of the internal energy of a system and the product of its pressure and volume (which expresses the work done against the external pressure). It is very difficult to measure, but in reality, when measured at constant pressure, represent the energy transfer, which is really important in the description of a system.

2.2   Pressure-enthalpy diagram

This diagram is a figure where, on the vertical axis, the absolute pressure is put, while in the horizontal axis the specific enthalpy can be found. They are used to represent refrigeration cycles, since they determine the limits in which a substance is found in a specific state. They are done for the refrigerant that is going to be used in the cycle. A representative diagram with the most important concepts to know about it is shown in Fig. 2.2.1.
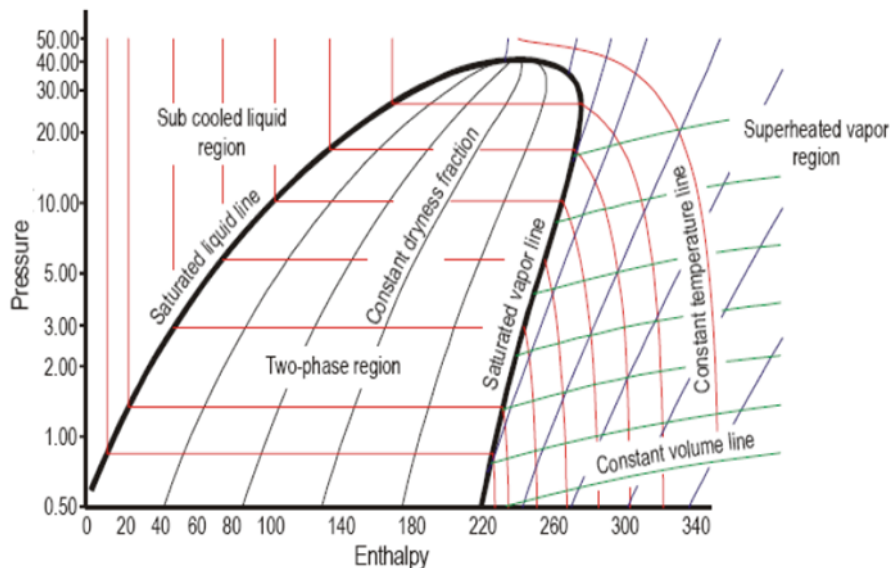

Figure 2.2.1: Concepts related to a pressure-enthalpy diagram [4]

There are many lines in this graph, each of them representing a constant property and, with the proper reading of these, provide information regarding the state of the fluid at study. The first characteristic line observed in one that has the shape of an upside-down U, and it represents the saturation line, which is a line that connects all the conditions of pressure and specific enthalpy that, when achieved, will cause to start the phase change. The left vertical curve represents the saturated liquid curve, while the most right vertical curve represent the saturated vapor curve. They meet at what is denoted as critical point, which is the point above which no additional pressure will cause a phase change from vapor to liquid. It divides the graph into three regions: liquid on the left, vapor on the right and a region known as two-phase in the middle.

- Liquid region or sub-cooled region: here, vertical temperature lines, which increase with the increase of enthalpy, are found. In this area, regardless of pressure, enthalpy or temperature, all of the fluid is found in liquid state.

- Vapor region or super-heated region: where vertical temperature lines that increase with the increase of enthalpy are found. Contrary to the previous case, in this region, the totality of the mix is found in gas state.

- Two-phase or mix region: in this zone, temperature lines are not vertical, but rather horizontal, which means that the transformation from one phase to the other is isothermal. This is because, while in this region, the addition of enthalpy will cause more and more liquid to vaporize, instead of increasing the temperature of the fluid.

Within the dome, vertical curves that indicate the vapor quality of the mix, x, are found. The vapor quality of the mix indicates which percentage of the mix is found in liquid state and which one is found in vapor state. The saturated liquid line has a quality of x=0, because the totality of the mixture is found in liquid state, while the super-heated line has a quality of x=1, as the totality of the mix is found in vapor state.

There are some lines that go above the dome, and never go inside of it. This indicates that, for those temperatures, the fluid will not change into liquid, it will always stay in vapor state.

2.3   Ideal, perfect and real gas

Although gas is state matter by itself, the theoretical representation of it can add some simplifications for an easier analysis. Therefore, there are many kinds of gases, that have different properties and make them more suitable for analysis, or more similar to the reality.

The three kinds of gases that exist are:

- Ideal gas: in this definition of the gas its particles are point particles, meaning they have no volume and that all of their mass is concentrated in a single point. Additionally, there is no inter-particle interaction between them. The advantage of this definition is that it obeys the ideal gas law, which is a simplified equation of state. Even though this is an approximation, this equation provides really good approximations of the behaviour of a real gas under many conditions.

- Perfect gas: it is an ideal gas whose specific heat capacities at constant volume (c_P) and at constant volume (c_V) are constant. This implies that their internal energy and enthalpy are linearly proportional to temperature.

- Real gas: the one that deviates from the ideal gas behaviour in due to the effects that the presence of non-point particles generate: having volume causes interaction between them. The adapted equation in this case is the Van der Waals equation.

In this paper, the refrigerant is going to be tested with these three definitions of a gas. When modelling these gas models in the Simescape environment [8], these different types of gas are defined as:

- Ideal gas: which is named as "perfect gas" in Simescape, where the coefficients that describe the gas are constant.

- Perfect gas: which is named as "semi-perfect gas" in Simescape, where the values of the coefficients that define the gas are a function of the temperature.

- Real gas: which is named as "real gas" in simescape, where the values of the coefficients that define it are a function of temperature and pressure. In this case, there are two tables that are used to model the real fluid:

  1. One table contains all the real coefficients of the fluid even when there is no phase change.

  2. Another table where the values of the coefficients for the liquid phase are forced to have the same value as the saturation conditions, in order for the ejector to still operate even when the fluid supposedly is in liquid phase.

It must be stressed that, regardless of the table chosen to model the "real gas model", there is no phase change in the fluid, to be in agreement with the model limitations.

All of these values will be displayed and further detailed in subsequent sections.

2.4   Incompressible and compressible flow

The increase in speed of a fluid can cause its particles to concentrate more, thus increasing the mass per unit volume or density. This is only noticeable at high speeds, and it is agreed that any fluid with a mach number Ma below 0.3 is incompressible, and above this value it is considered compressible. This is very important, because the main difference between these regimes lays on the fact that the density of the fluid can be considered constant (in the case of the incompressible fluid) or not.

2.5   Subsonic and supersonic flow

The speed of a fluid can also lead to another regime distinction, depending on the ratio between this speed and the speed of sound. This ratio is called Mach number, Ma, and it a fluid has a speed below the speed of sound ($Ma < 1$), it is said to be in subsonic regime. If the speed is above the speed of the sound ($Ma > 1$), it is said to be in supersonic regime.

Being in a regime or another implies a big difference in how the fluid behaves. When a fluid is reaching the speed of sound, there is a pressure buildup, which poses an increased difficulty in the advance of the fluid, known as sound barrier. When this limit is overcome, shock waves are created, which are pressure waves that propagate at speed higher than the sound. They generate a big disturbance in the medium.

These may seem uncommon, but in any environment where there is an increase in speed there is risk of these appearing. One example is inside a nozzle, which is a mechanical device with

varying cross section used to accelerate or decelerate a flow, depending on how the variation of cross-sectional area occurs. This occurs due to Venturi´s effect, which states that upon the reduction of the cross section (convergent) of the area through which a fluid circulates, it increases its velocity, thus generating a pressure reduction. The opposite occurs with an increase of the cross-sectional area (divergent), which reduces the velocity of a fluid and increases its pressure.
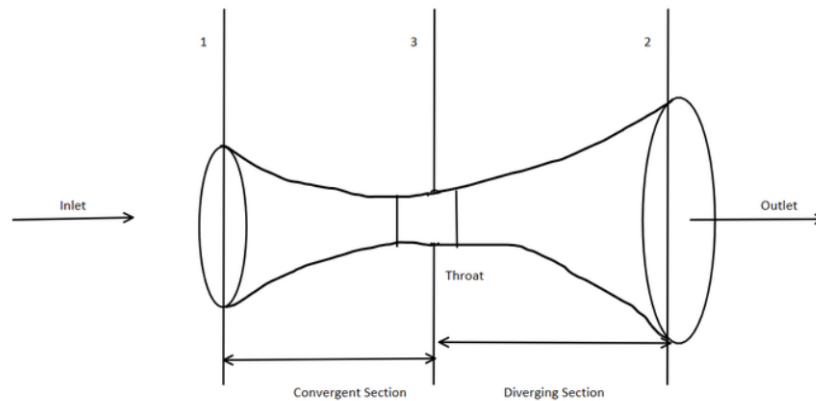

Figure 2.5.1: Convergent-divergent nozzle [10]

A very common type of nozzle is the convergent - divergent one (Fig. 2.5.1), there the part with the smallest area is called the throat. This is the point where the fluid reaches the maximum velocity and, in many cases even if the entrance and outlet speed are well below the speed of sound, it may occur that in the throat the flow is accelerated to speeds above it. Additionally, when the speed of the fluid increases too much, the flow can become chocked. Chocked flow is related to the Venturi effect. The increasing velocity of a flow causes a decrease in the pressure of the same in order to fulfill the conservation of energy principle. But a significant increase in the velocity will also eventually affect the density of the fluid by decreasing it. In order to conserve the energy, mass flow must increase. However, this increase is not unlimited, but in fact has a maximum value. When this point where the density of the fluid continues to decrease but is not accompanied by as increase of the mass flow is when the fluid becomes chocked.

2.6   Refrigeration cycle

Refrigeration cycle, also sometimes referred to as heat pump cycle, is a thermodynamic and mechanical process by which heat is extracted from a high temperature source into a sink, with the goal to evacuate the heat from the system and to therefore reduce the temperature of said source. A thermodynamic cycle is a process by which a system undergoes changes in some of

its physical parameters, such as temperature, volume or pressure, but in the end the final state of it is the same as the initial one, therefore its net change in state is null. There are many types of refrigeration cycles, all of them with their own working principles. The most common ones are:

- Compression refrigeration cycle:

  Also known as vapor compression refrigeration cycle, it is based on changing the state of the cooling fluid from liquid to vapor and vice-versa. This allows the refrigerant to absorb heat from the surroundings (when it evaporates), and thus generate the cooling desired. A basic scheme of this process can be observed in Fig. 2.6.1.

  The compressor has as an input refrigerant in vapor state at low pressure, and is when it goes through this element that it increases the value of the pressure and the temperature. This vapor enters the condenser, where it exchanges heat with the outside of the system, thus releasing it to the outside environment and removing it from the system. This causes the refrigerant to loose temperature and condensate into a saturated liquid, but still maintain a high pressure. In order to decrease it, the fluid goes through an expansion valve, where the abrupt pressure decrease causes the fluid temperature to go further down and to eventually fully condensate. This liquid now goes to the evaporator, where it will absorb heat from the source. This will cause it to increase its temperature and to eventually evaporate, thus restarting the cycle.
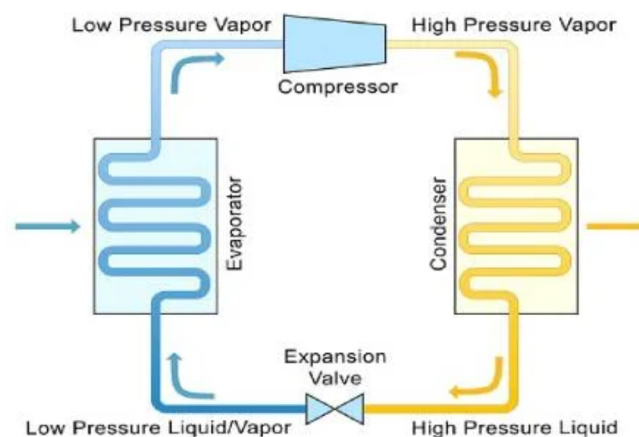

Figure 2.6.1: Basic elements of a compression refrigeration cycle [3]

- Absorption refrigeration cycle:

  This type of refrigeration cycle is fairly similar to the compression one, for it uses a refrigerant with a really low boiling point, so that when it evaporates, it absorbs heat from the surroundings and thus cools them down. The main difference with respect to

the compressor refrigeration is that this gas is changed into a liquid again, so that the cycle can start again. This is done by employing an absorber. Notice that there is no compressor element in this type of cycles. The basic structure can be observed in Fig. 2.6.2.

In the evaporator, the refrigerant absorbs heat from the environment, which causes it to evaporate while cooling the medium down. Because it has a low partial pressure, the evaporation temperature is also low. This goes into the absorber, producing a refrigerant-saturated liquid that flows into the next step. Regeneration is when the refrigerant-saturated liquid is changed into liquid again so that it can be reused. This is done without using any mechanical parts, but only with gravity. The evaporation occurs at the lower end of a narrow tube, so that when the refrigerant evaporates, it causes the bubbles to rise and push the liquid into a higher chamber, from which it will fall (due to gravity) into the absorption chamber,thus reentering the cycle. As for the evaporated refrigerant, it will eventually pass through an environment with lower temperature, such as the ambient one, which will cause it to condense and fall into the supply for the evaporation phase.
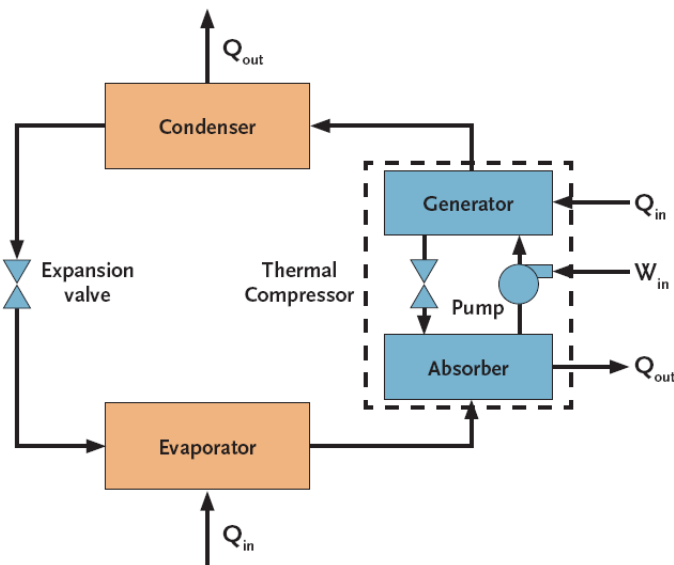

Figure 1 Basic absorption cycle

Figure 2.6.2: Basic elements of an absorption refrigeration cycle [6]

2.7 Ejection refrigeration cycle

This refrigeration cycle is characterised by having an ejector, which is in charge of recovering part of the wasted heat, allowing it to reenter the cycle and increasing its efficiency. The basic structure of this refrigeration cycle can be observed in Fig. 2.7.1.
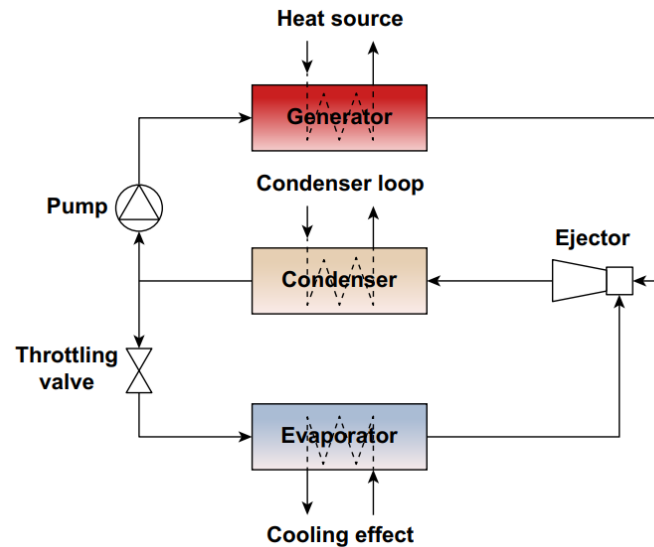
Figure 2.7.1: Basic elements of an ejection refrigeration cycle [13]

This cycle can be defined as two closed cycles or loops that are connected through the condenser and the ejector: high pressure loop and low pressure loop. The purpose of each of these is:

- High pressure loop:

  - Pump: pushes part of the fluid that comes out of the condenser to the generator.

  - Generator: is where the pushed fluid absorbs the residual heat from a source and increases its pressure and temperature. This is what creates the primary flow that will enter the nozzle of the ejector.

- Connecting leg:

  - Ejector: the primary flow enters and absorbs the secondary flow, which comes from the evaporator. They mix at an intermediate pressure and temperature, and leave the ejector at increased pressure, caused by the diffuser.

  - Condenser: the mixture enters this heat exchanger, where it releases heat to the outside, removing it from the refrigeration system. Here, the fluid theoretically transitions to liquid state, but in reality many times it is a gas with droplets, called saturated liquid. It has a lower temperature and pressure, and is divided into two streams: one returns to the high pressure loop though the pump, while the other one goes to the expansion valve.

- Low pressure loop:

- Throttling or expansion valve: it causes an abrupt pressure drop of the saturated liquid, which will ensure a full transition to liquid state at a low temperature into the evaporator.

- Evaporator: here, the liquid evaporates by absorbing heat from the medium that is desired to cool down.

2.8   ph diagram of the ideal gas ejection refrigeration cycle

As previously mentioned, a ph diagram is used to represent a refrigeration cycle. Now that the cycle which uses a jet ejector has been introduced, it is interesting to analyse in over this kind of diagram, which will allow for a more complete understanding of the same.

In Fig. 2.8.1, the cycle has lines of three different colors: red for the primary flow, green for the secondary flow and blue for the mix.

Analysing starting at the separator (6G) towards the high-pressure loop, it can be observed that the flow that reenters the cycle is the one in vapor state. When it goes through the compressor (2), it increases its temperature and pressure, which makes it go deeper into the vapor zone (the right side of the graph). Then, it goes through the condenser (3), where it releases heat and condensates, which makes it change into liquid state, and thus moves to the left side of the dome (saturated liquid line). When it enters the ejector (4), due to the nozzle, its pressure is reduced, thus the decrease in the dome. Notice that now, because of this pressure decrease, the fluid will be partially in liquid state and partially in vapor state.

As for the low-pressure loop, it starts at the separator (6L), but on the opposite side of the dome, because the fluid that is used is in liquid state. When it through the throttle or expansion valve (7), it expands, which decreases its pressure slightly, which in the ph diagram is represented by a vertical line downwards. Same as in the nozzle, the fluid now is found within the saturation dome, so there is a mix of vapor and liquid. After exiting the evaporator (8), the fluid had absorbed heat and evaporated, and this is represented by shift to the right of the dome. When it is sucked inside the ejector (9), its pressure is somewhat reduced to the same value that the primary flow has. They combine in the mixing chamber (5), and reach an intermediate value of entropy. Lastly, when exiting the ejector due to the presence of a diffuser to equalise the pressure of the mix with the outside, its pressure increases (6), and the cycle restarts.
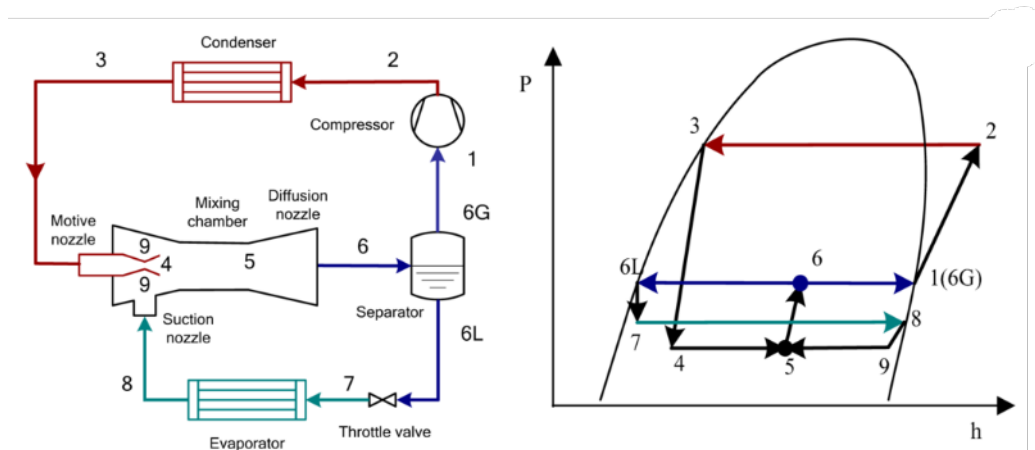
Figure 2.8.1: ph diagram of an ideal jet ejection refrigeration cycle [12]

2.9   Ejector

An ejector or vacuum ejector is a vacuum pump that, utilising the Venturi effect utilizes a high-pressure fluid flow (primary flow) to absorb and compress a low-pressure fluid flow (secondary flow). It is this what generates the vacuum that absorbs the secondary flow into the piece.

In refrigeration systems, ejectors are used to increase the pressure of refrigerant vapor before it enters the condenser.

2.9.1   Geometry and working principle

A CAD of what an ejector looks like can be observed in Fig. 2.9.1, and, depending on the process in which it is placed, the dimensions of it change. Also, depending on the operational environment of the piece, its optimal design will differ. Nevertheless, the same basic structure is present in all the pieces.
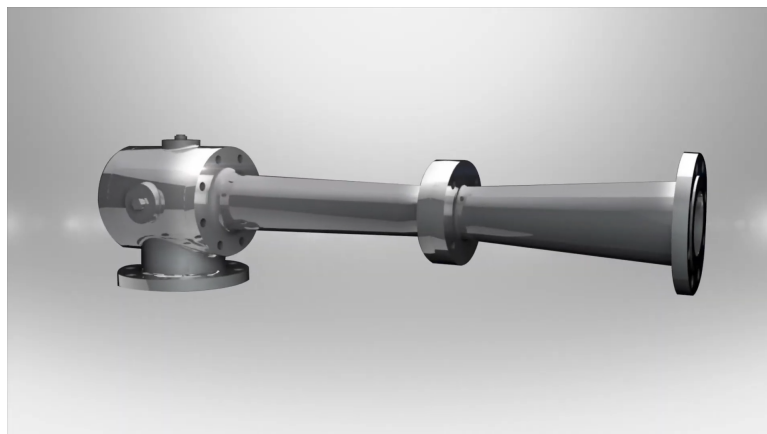

Figure 2.9.1: CAD of a jet ejector piece [1]

Nevertheless, all of the pieces have the same basic internal structure, which is represented in Fig. 2.9.2, together with all the different geometrical parameters that determine the design

as well as the distribution of the fluids inside of it. The geometrical parameters play a crucial role in the process, since they determine the nozzle and diffuser geometry. Varying these, the most optimal geometry for each case can be determined, and is particular to each process. This is advantageous in the sense that, for some operating conditions, a perfectly tailored piece can be manufactured to ensure optimal performance. However, a geometry is only optimal for the design operating conditions, and if the process that is undergoing is not within the reference values, the general efficiency of the cycle can be severely reduced. In order to generate the model of the piece, many of these values are going to be defined, and this will be displayed in Section 3
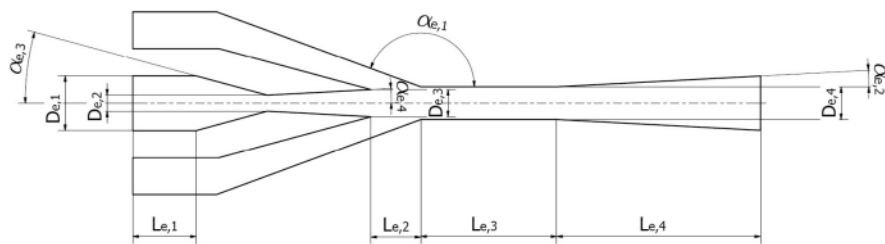
(a) Internal structure of an ejector [5]
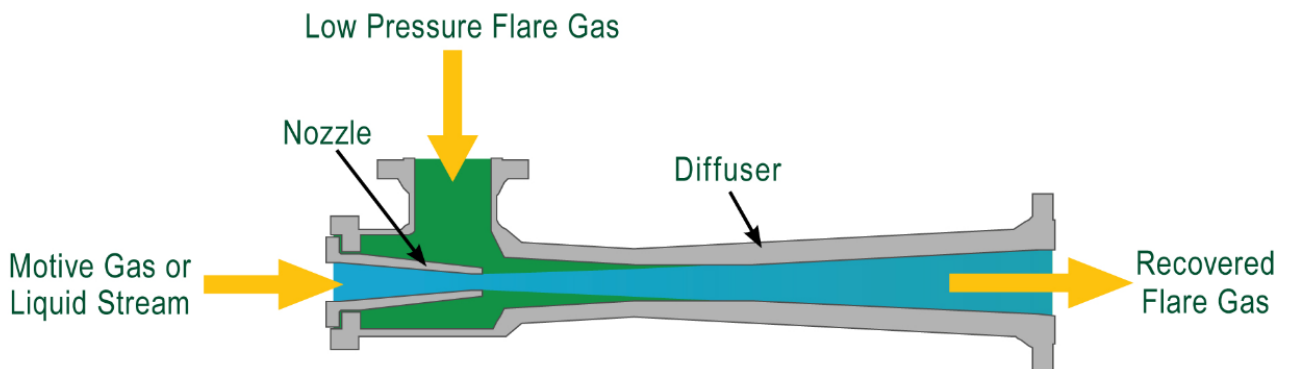
(b) Fluid distribution inside an ejector [11]

Figure 2.9.2: Geometry and internal fluid distribution of a jet ejector

In these images, the first one represents the geometrical parameters that can be used to design and optimize an ejector, and the figure utilised to illustrate this corresponds to a supersonic ejector, since it has a convergent-divergent nozzle. The second image, which is used to illustrate the distribution of fluids inside the piece, is illustrated using a subsonic ejector, since it has a convergent nozzle. They are not the same type of ejector, but they represent essentially the same process.

The ejector has two input ports: the central channel and one (or two) lateral ones. Through the central channel flows what is denoted as *primary flow*, which is the one that has received

energy from a heat source, like a generator. Using Venturi effect, in the nozzle, this primary flow is accelerated so that when it arrives at the mixing chamber it has a pressure that is low enough to create vacuum, which will absorb what is denoted as the *secondary flow*. This flow is a fluid that has lower temperature and lower pressure, and it the one that generates the cooling capacity, for it absorbs heat from the medium to be cooled. These flows start to mix in the mixing chamber, but continue doing so also along the exit channel, ensuring the most homogeneous blend, generating a third flow that has an intermediate pressure. At the end of said channel, there can be found a diffuser, which is used to equalize the pressure of the mixed fluid with the one of the surrounding by slowing it down, which increases its pressure (following the same Venturi effect as the nozzle, but in the opposite way).

2.9.2   Characteristic parameters

With the aim of understanding and determining the operational ranges of an ejector, the following mathematical variables and characteristic parameters are created [5]:

- Entrainment ratio, ω, which is mathematically defined as:

$$\omega = \frac{\dot{m}_S}{\dot{m}_P} \tag{1}$$

  It defines the relationship between the fluid mass flow of the secondary flow with respect to the primary flow. It is one of the most important parameters in the definition of an ejector.

- Primary pressure ratio, Π_{po}, which is mathematically defined as:

$$\Pi_{po} = \frac{p_{outlet}}{p_P} \quad \epsilon \quad [0,1] \tag{2}$$

  It defines the relationship between the outlet pressure with respect to the pressure of the primary flow.

- Secondary pressure ratio, Π_{so}, which is mathematically defined as:

$$\Pi_{so} = \frac{p_S}{p_{outlet}} \tag{3}$$

  It defines the relationship between the pressure of the secondary flow with respect to the outlet pressure. It has the opposite structure with respect to the primary pressure ratio so that its value is also constrained within 0 and 1 but, in this case, considering that there are point when the secondary pressure is higher than the outlet one, the ratio will take values above 1.

2.9.3   Operational regimes

As previously mentioned, an ejector is intended to have the best operation. Nonetheless, due to all the physical phenomena that occur inside of it, the values of the different physical variables pose a big influence on this. The most important and characteristic one is the pressure, most specifically the pressures of the primary fluid, the secondary fluid and the outlet fluid. Analysing the values of these, three different operational modes are differentiated:

- Double-chocking (critical mode): This is the desired operation mode, and is characterized by the fact that both the primary and the secondary flow both reach supersonic conditions and become chocked. Additionally, for a given and constant value of p_P, the entrainment ratio ω is independent of the ejector back pressure, which implies that both of the mass flows increase together or they are constant.

- Single-chocking mode (subcritical mode): This operational mode is characterized by the fact that the minimum critical back pressure is exceeded, meaning that the outlet pressure is below the minimum value, and therefore it can lead to one of the flows (or none of them) being chocked. This generates oblique shock waves inside the channels, which has several negative effects, including disturbance of the mixing process as well as interference with the suction of the secondary flow, thus reducing the secondary mass flow and, as a consequence, of the entrainment ratio. This regime should be avoided, especially when considering the sensitivity of the ejector to fluctuations of the back pressure.

- Backflow mode (reverse mode): This regime is similar to the previous one, but in this case both flows are disturbed, not only the primary one. When the back pressure is exceeded, a secondary shock wave moves upstream, affecting the entrance of the primary flow. This has a consequence of inadequate expansion of the same, which in turn affects the suction of the secondary flow, causing a drastic decrease in ω below 0, meaning that the mass flow flows in the opposite direction. This is a malfunction mode and should be avoided.

The two-dimensional plot that will be used to analyse the effect of the efficiencies is one where the entrainment ratio will be plotted against the secondary pressure ratio, for three different values of the primary pressure ratio, as shown in Fig. 2.9.3.
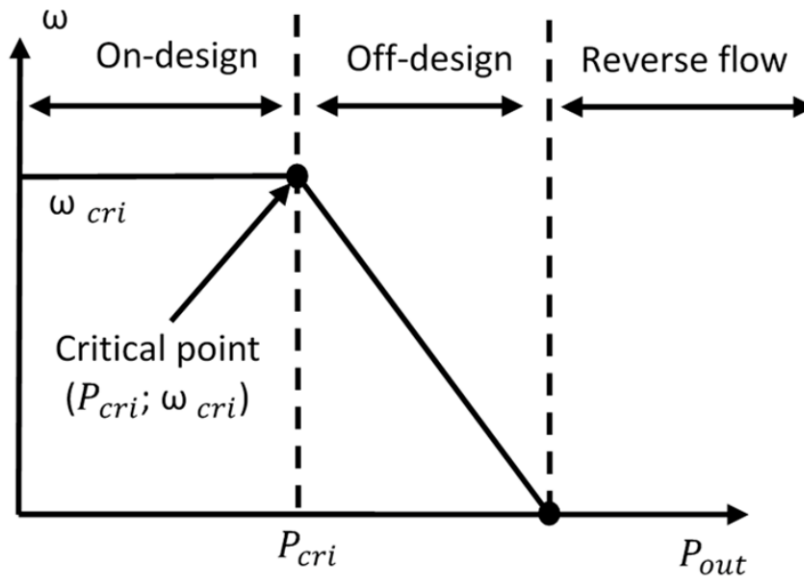
Figure 2.9.3: General two-dimensional plot for the operating regimes of an ejector

All of these modes can be graphically represented using the performance map of an ejector [5]. This is a plot in which the entrainment ratio ω is plotted against the operating pressure ratios Π_{po} and Π_{so}. Based on the physical phenomena that characterise each operating mode, the surface of the performance map has a defined tendency. These tendencies are:

- Critical mode: it is graphically represented by a surface that is proportional to both pressure ratios, meaning that the entrainment ratio increases if any of the pressure ratios increases, which implies the increase of the primary or secondary pressures alone, considering the fact that the back-pressure has a constant fixed value.

- Subcritical mode: in this case, the presence of shock waves affect the mixing process and therefore the entrainment of the secondary flow while the primary mass flow is chocked. As a consequence, this is represented a a decrease in the entrainment ratio as the secondary pressure ratio decreases, which is seen as a plane with a decreasing slope in that direction.

- Backflow mode: it implies that the entrainment ratio has a negative value, therefore in the performance map it is illustrated when the surface crosses the horizontal plane and goes to negative values.
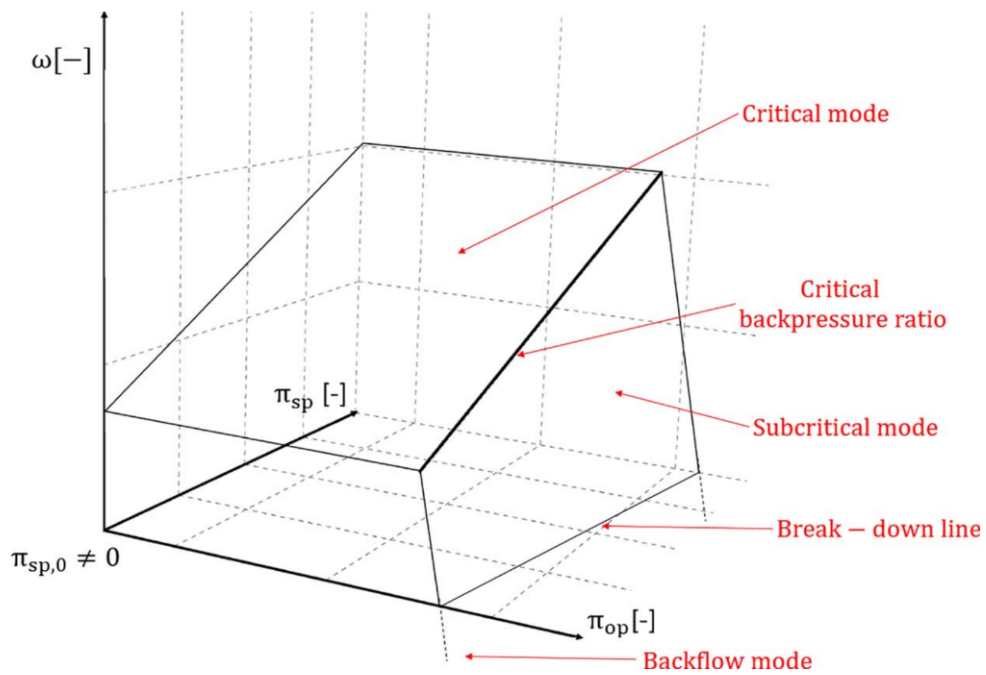
Figure 2.9.4: Characteristic surfaces of the performance map of an ejector [5]

3 Matlab

To perform the simulation of all the necessary cases, a simescape model of an ejector piece in Matlab was utilized. In this section of the paper, a detailed description of the same is performed, analysing not only the block that compose it but also the settings of each one of them. Additionally, the usage of three different gas models is required, therefore they also are defined. Important to note that this model was developed by the tutor of this project, Vicente Dolz, being him the ones who chose the values of the constants of the gases, as well as developed the tables employed for the modelling of the real gas.

3.1 General structure of the model

The general structure of the simulation consists of the ejector piece in the center, with three channels that simulate and determine the characteristics of the primary, secondary and resultant flow. Each of them has a defined temperature and pressure, which define the conditions of the controlled reservoir block, in charge of defining the boundary conditions of the model. Next, an "S-block" which is in charge of obtaining the different variables at study of the gas is found. On the outlet of the piece, the block that models all of the gases utilised is found, and can be changed between the real gas and the perfect gas. Last but not least, the configuration of the solver that runs the simulation is found.

To display the calculated values, a scope block is employed, which is used to display the six different signals of interest, which are obtained from the "S-block" of each flow.
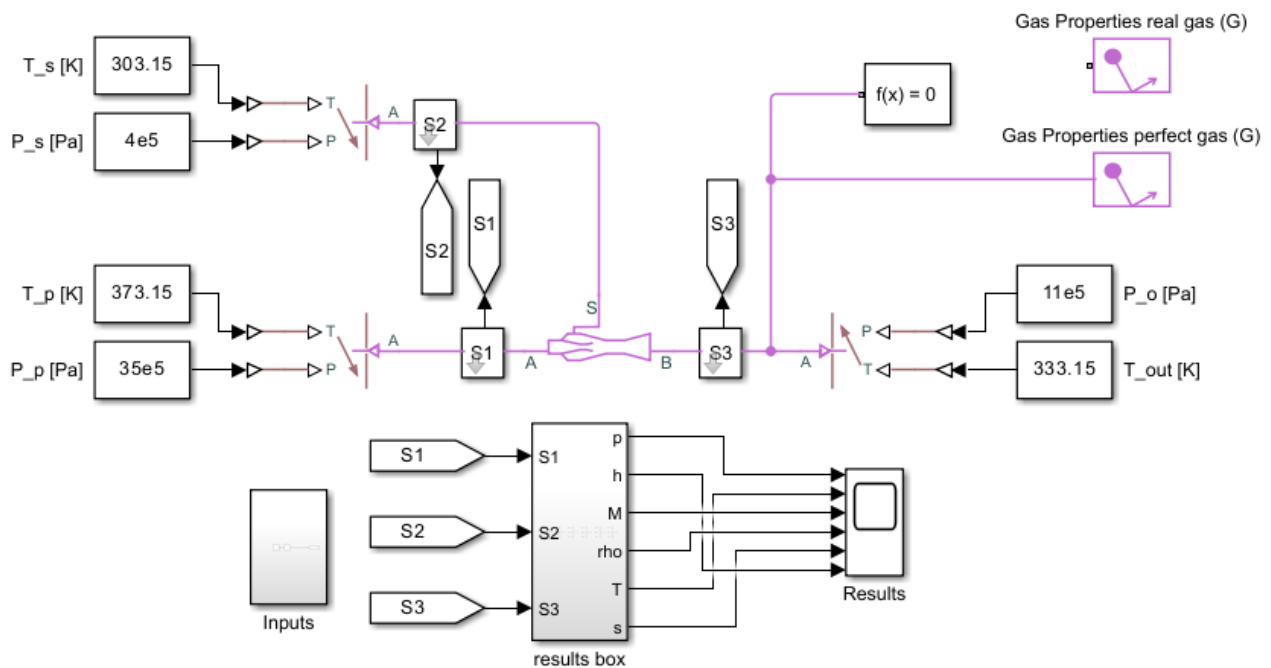

Figure 3.1.1: General structure of the model

3.2   Definition of each element

In this part of this section, a more thorough description of each block and the parameters that define it will be done.

- Controlled tank reservoir

  This elements is in charge of setting the boundary conditions of the fluid in a gas network. The gas enters the reservoir at the set pressure, and leaves at the set pressure and set temperature. However, it enters the tank at a temperature that is calculated using gas properties, based in the inlet pressure. The values of pressure and temperature are set using constant blocks.
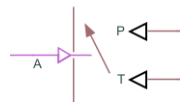
Figure 3.2.1: Controlled reservoir block

  The configuration required for this elements is simple, consisting of only the cross sectional area of the ports.

Parameter	Value	Unit
Cross sectional area of port A	0.01	m^2

Table 3.2.1: Controlled reservoir configuration

- S block

  This block's goal is to collect and contain all the sensors that are used in this analysis. All the values obtained are sent to be displayed using a "goto" block.

Figure 3.2.2: S-block

  When clicking on the subsystem, it opens up and displays what can be seen in Fig. 3.2.3.
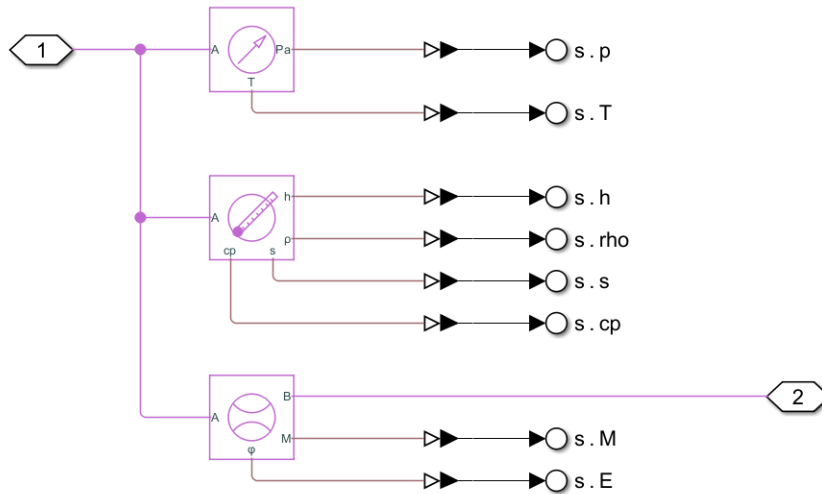
Figure 3.2.3: S-block sensors disposition

The sensors that are found are:

– Pressure and temperature sensor

 As its own name indicates, it measures the pressure and temperature of the gas inside a gas network. There is no mass or energy flow inside the sensor. In the pressure measurement, it can set as a reference both an absolute value of the pressure of a difference, for the posterior measurement of either the absolute pressure or the gauge pressure. In the temperature measurement, it directly measures its value across the sensor.
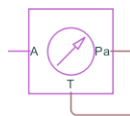
Figure 3.2.4: Pressure and temperature sensor block

Parameter	Selected
Measurement reference	**Absolute**
	Difference
Pressure type	**Absolute**
	Gauge

Table 3.2.2: Configuration for the Pressure-Temperature sensor

– Thermodynamic properties sensor

 This block measures the main thermodynamic properties (specific enthalpy, density, specific heat and specific entropy) in the sensor, through which there is no mass or

energy flow. The options that can be selected, and that were in fact selected in this case, are displayed in Table 3.2.3.

Parameter	Selected
Enthalpy	X
Density	X
Specific heat	X
Entropy	X

Table 3.2.3: Configuration for the Thermodynamic properties sensor

The only setting necessary is setting the value of the specific entropy (3.8635 $\left[\frac{kJ}{kg \cdot K}\right]$) at the reference pressure (101325 [Pa]) and temperature (293.15 [K])

Parameter	Value	Unit
Reference temperature	239.15	[K]
Reference pressure	0.101325	[MPa]
Specific entroypy	3.8635	$\left[\frac{kJ}{kg \cdot K}\right]$

Table 3.2.4: Selection of the Thermodynamic properties sensor reference values
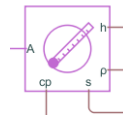
Figure 3.2.5: Thermodynamic properties sensor block

– Flow rate sensor

It is responsible for measuring the flow and energy rate across the system, which are not taken into account in the aforementioned sensors.

Parameter	Selected
Mass flow rate	X
Volume flow rate	
Energy flow rate	X

Table 3.2.5: Selection of the flow rate sensor reference parameters to analyse
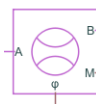

Figure 3.2.6: flow rate sensor block

- Input block

  This block is not used in this project, but if it were to be used, its goal would be to change the boundary conditions, in order to analyse how the change of these would affect the performance of the piece.

Figure 3.2.7: Input block

- Solver

  This is the processing unit of the simulation, and is in charge of solving it. To configure it, some parameters such as the system variable, in this case the time, the tolerance factor, of 0.001 in this case or which solver to use are defined. All of these settings can be observed in Fig. 3.2.9
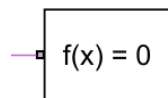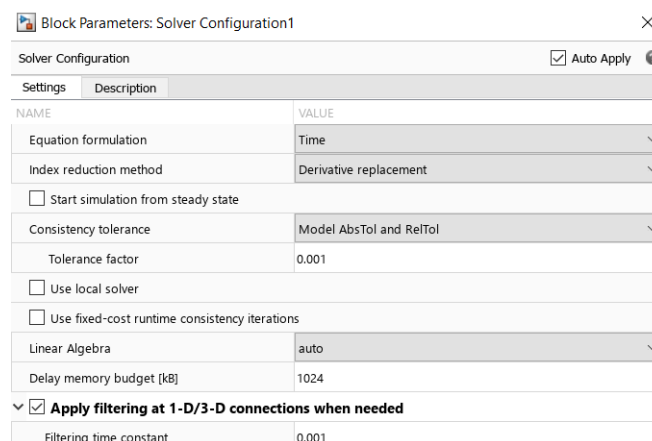

Figure 3.2.8: Solver block

Figure 3.2.9: Solver configuration

- Results

  This part of the model is the responsible for displaying the obtained values. They use as an input the values of the parameters taken at the different S-block sensors, which are sent using the "*goto*" block.
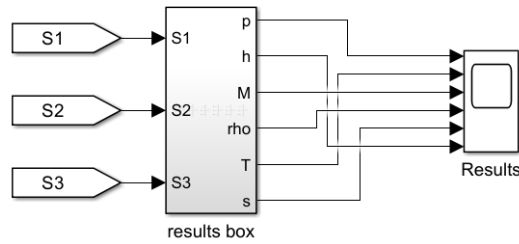
Figure 3.2.10: Results box

When clicking inside the results box, the variables arrangement can be seen, where each variable for each fluid of the system are organized so that they can be displayed in a more arranged way.
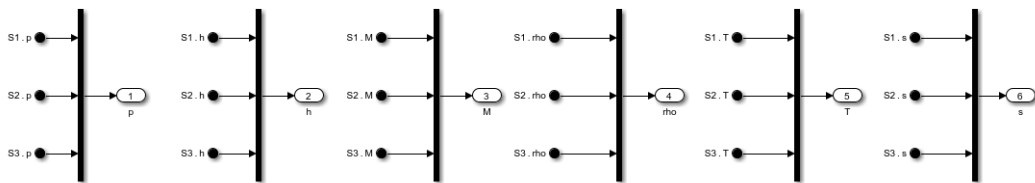

Figure 3.2.11: Content of the results block

With the purpose of showing how the results display scope block looks like, the base case was run, and its results display can be observed in Fig. 3.2.12.
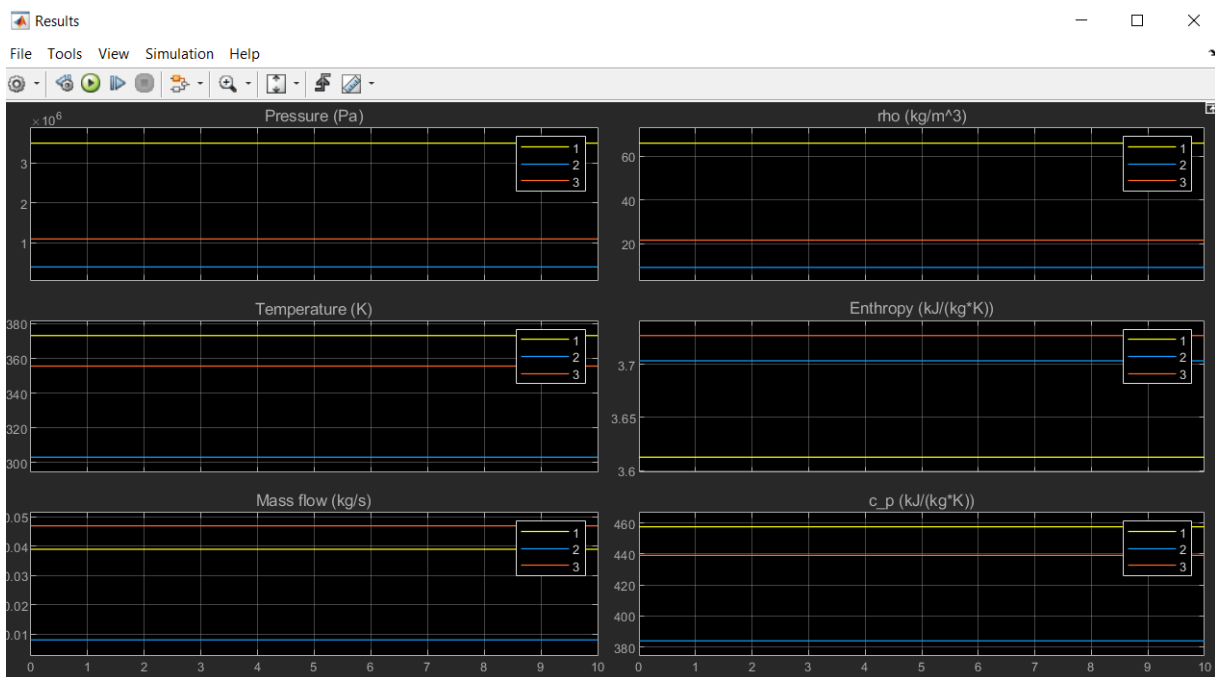

Figure 3.2.12: Display window of the results

- Ejector

This is the central element of this paper. Its block looks like what is shown in Fig. 3.2.13, and it can be seen that, through port A is where the primary flow enters, while the secondary flow is the one that enters through port S. The mixed final flow, which is assumed to be under uniform pressure , exits the piece through port B.
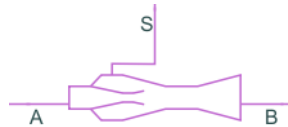

Figure 3.2.13: Ejector block

To define it, there are two different necessities: determining the geometrical parameters and geometrical ratios, and determining the efficiencies of the different processes that occur inside, with the aim of making the model as accurate and realistic as possible.

Parameter	Value	Units
Primary nozzle throat area	4.227	[$mm^2]
Area ratio of nozzle exit to throat	2.085	[-]
Area ratio of mixing chamber to throat	5.99	[-]
Minimum area ratio of secondary throat to primary throat	0	[-]
Efficiency for primary flow through nozzle	0.9	[-]
Efficiency for secondary suction flow	0.85	[-]
Efficiency for primary flow expansion	0.85	[-]
Efficiency for mixing	0.8	[-]
Cross-sectional area at port A	2	[$cm^2]
Cross-sectional area at port S	2	[$cm^2]
Cross-sectional area at port B	2	[$cm^2]

Table 3.2.6: Configuration of the ejector model

In order to understand how matlab modelled this piece, in Fig. 3.2.14 it can be seen where each variable that appears in the equations, as well as what each geometrical parameter is.
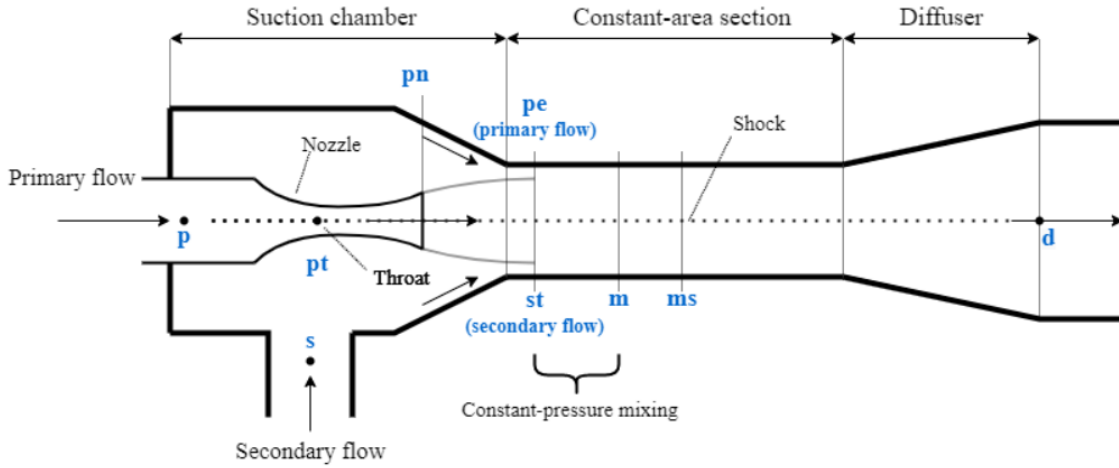
Figure 3.2.14: Matlab geometrical definition of the ejector

– Geometrical parameters:

The optimal geometry for a given operational environment varies depending on the conditions. In this case, the values chosen are:

* Primary throat area $[S_{PT}]$ (4.224 $[mm^2]$): this is the nozzle that decreases the pressure of the primary flow in order to generate the vacuum that will suck in the secondary flow.

* Area ratio of nozzle exit to throat (2.085): this means that the nozzle exit cross sectional area is roughly twice as big as the throat. This determines the amount of expansion the flow experiences, and therefore the secondary flow mass rate that is sucked in.

* Area ratio of mixing chamber to throat (5.99): in this case, the mixing chamber is almost a sixfold of the throat area

* Cross sectional area of each port (2 $[cm^2]$).

– Efficiencies:

They determine what percentage of the flow is lost along these processes due to reality imperfections such us friction, imperfect mixing, uneven pressure distributions or others, with respect to the ideal scenario. All these values are empirically determined, and the ones displayed are the ones corresponding to the base case, which will be altered for the posterior parametric study.

* Efficiency of the primary flow through the nozzle ($\eta_P = 0.9$): it accounts for the primary flow rate reduction due to the losses in the primary nozzle, due to losses like friction. It has a direct effect on the primary mass flow, as it can be seen in the equation that the model uses to calculate it:

$$\dot{m}_P = S_{PT} \cdot \sqrt{\frac{2\gamma}{\gamma-1}\eta_P p_P \rho_P \left[\left(\frac{p_m}{p_p}\right)^{\frac{2}{\gamma}} - \left(\frac{p_m}{p_p}\right)^{\frac{\gamma+1}{\gamma}}\right]} \qquad (4)$$

∗ Efficiency for the secondary flow suction ($\eta_S = 0.85$): it accounts for the losses in the secondary mass flow due to friction and others. Its effect on the secondary mass flow into the ejector can be easily observed in the equation that defines this value:

$$\dot{m}_S = S_{ST} \cdot \sqrt{\frac{2\gamma}{\gamma-1}\eta_S p_S \rho_S \left[\left(\frac{p_m}{p_s}\right)^{\frac{2}{\gamma}} - \left(\frac{p_m}{p_s}\right)^{\frac{\gamma+1}{\gamma}}\right]} \qquad (5)$$

∗ Efficiency for the primary flow expansion ($\Psi_{pe} = 0.85$): it accounts for the decrease of the predicted expansion area of the primary flow, which is how much the primary flow expands when exiting the nozzle.. This can be observed in the mathematical relationship that defines it:

$$\frac{S_{pe}}{S_{pt}} = \Psi_{pe} \sqrt{\frac{\left(\frac{\gamma-1}{2}\right)\left(\frac{2}{\gamma+1}\right)^{\frac{\gamma+1}{\gamma-1}}}{\left(\frac{p_m}{p_p}\right)^{\frac{2}{\gamma}} - \left(\frac{p_m}{p_p}\right)^{\frac{\gamma+1}{\gamma}}}}$$

∗ Efficiency for the mixing ($\Psi_m = 0.8$): it accounts for the losses of mixed flow velocity, which comes from the momentum balance equation. This has an effect on the velocity of the mixed fluid, as can be seen in the following mathematical expression:

$$v_m = \Psi_m \frac{\dot{m}_P v_{pe} + \dot{m}_S v_{st}}{\dot{m}_m}$$

This model presents several assumptions and limitations [7], being the two most relevant ones:

∗ Inaccurate results when working in reverse flow conditions.
This is caused due to the fact that the model assumes isentropic flow throughout the whole ejector, including some efficiencies to make the results closer to the real case. Also, if necessary, it models one normal shockwave in the mixing channel. When working in reverse flow conditions, there may be more shock waves that are not modelled, which reduces the accuracy of the results.

∗ Working fluids must be found completely in gas state.
In order to comply with this limitation, what is done is that the tables of thermodynamic parameters values that define the fluid for different combinations of

temperature and pressure values, are forced to take the saturation value when the fluid is found outside of this region. This causes that, when the fluid is outside of the saturation region, the results are less valid, for the parameters that define them are not the real ones. That is also why the properties library that is embedded in simescape is not useful.

These two limitations are the ones that drive this study, but this model has additional assumptions and limitations:

∗ Gas flow is assumed to be isentropic, steady, one-dimensional and adiabatic.

∗ The use of empirical coefficients is what accounts for the losses of the model (friction, mixing and expansion).

∗ The flows do not mix until the primary flow has expanded completely.

∗ The two flows mix at constant pressure, after the primary flow expanded.

∗ The kinetic energies at the inlet of the primary flow, the secondary flow and at the diffuser outlet are neglegible compared to the kinetic energy inside of the ejector.

∗ The results with reverse flow may not be accurate.

3.3   Models of the operating gases

The configuration of the matlab model makes it incompatible with the presence of fluid in any other state than gas. The perfect and semi-perfect models work adequately under this hypothesis providing no errors. Nevertheless, the real gas does go beyond the saturation dome, reaching liquid state, which caused an error in the simulation. This was corrected by generating properties tables, which will be explained in detail in its corresponding section.

3.3.1   Perfect gas

For the definition of this gas is the simplest one, since the values of the constants do not vary with pressure nor temperature, therefore they are just a constant for all of the cases, so with the definition of a scalar is enough. In Fig. 3.3.1 the values of each of these variables can be observed. The choice of the parameters ensures that the gas is always in gas state, thus not posing any trouble to the simulation.

Reference parameter	Value
T [K]	303
p [MPa]	0.101235

Figure 3.3.1: Perfect gas configuration

Parameter	Value	Units
R	0.17062	$\left[\frac{kJ}{K \cdot kg}\right]$
Compressibility factor	0.835	[-]
h	382.72	$\left[\frac{kJ}{kg}\right]$
c_p	1.0522	$\left[\frac{kJ}{K \cdot kg}\right]$
μ	12.741	$[s * uPa]$
k	0.014281	$\left[\frac{W}{K \cdot m}\right]$

Table 3.3.1: Configuration parameters of the perfect gas

3.3.2   Semi perfect gas

In this case, the value of the parameters describing the gas depends on the temperature, therefore for all of these a vector array must be defined for every temperature. The choice of these values ensures that the gas never reaches the liquid side of the saturation dome, thus not posing any threat to the simulation. As for the pressure, it maintains a constant value.

Figure 3.3.2: Semi-perfect gas configuration

The values of the parameters employed for the simulation can be observed in Appendix A.1. These values were chosen for a pressure that ensured that, regardless of the fluid temperature, it would always be found in gas phase.

Using these temperature variant variables together with the embedded equations and thermodynamic properties tables that Simescape already has in its library, the gas can be calculated for the different simulation conditions.

3.3.3   Real gas

This model of the gas has the characteristic that the thermodynamic properties not only vary with the temperature, as in the previous case, but also with the pressure. It is for that reason that, as an input, the program requires not a vector but a matrix of values for each case of the thermodynamic variables.

Nevertheless, the library found within Simescape describing the R1234yf fluid was generating a problem in the simulation: it made the working fluid within the ejector go into liquid phase. It must be stated that this is not a problem, for the real values of the properties of the fluid are correct, it is just the simulation environment the one that can not handle this phase change.

Figure 3.3.3: Real gas configuration

Therefore, in order to keep a matrix of properties, but also ensuring that the model could compile adequately, there was an edit made to the tables. It consisted on forcing the values of

the properties that would make the gas liquid to have the same values as in the saturation line. In this way, the working fluid would be as realistic as possible and as close as allowable to the liquid phase, without compromising the integrity of the simulation.

The values given for each combination of pressure and temperature can be seen in Appendix A.2.

4 Results

This section is where the explanation of the process followed to obtain the mass flow rate of the primary and secondary flows for different ratios of primary, secondary and outlet pressures is described. After the collection of this data, the entrainment ratio and pressure ratios were calculated, for a later display in a 3D surface utilising Matlab.

The goal of this process is to asses how the matlab model behaves and operated when in reverse flow conditions in a qualitative manner, by comparing the actual results with the expected and real ones.

Additionally, the variation of each efficiency and gas model affects the ultimate results, taking as a reference a case the one previously described. To do that, the simplest case to study, the perfect one, will be analysed for the search of the effect of the efficiencies variation. Once this thorough process is completed, a comparison between the perfect cases and the semi-perfect and real ones will be done, looking for a conclusion on the effect that the gas model poses.

It must be highlighted that, in the rest of the literature, the plot has the opposite shape, because what is done is fixing both the primary and the secondary flow pressure, while varying the outlet pressure. In this case, however, considering that the fixed parameter is the outlet pressure while the others two are varied, the secondary pressure ratio behaves the opposite way, in the sense that increasing the outlet pressure decreases the secondary pressure ratio. Nevertheless, the regions in the plot coincide.

Another important remark to be made is that, for the ranges at study, the plot will only display the behaviour of the sub-critical and reverse flow operating regimes.
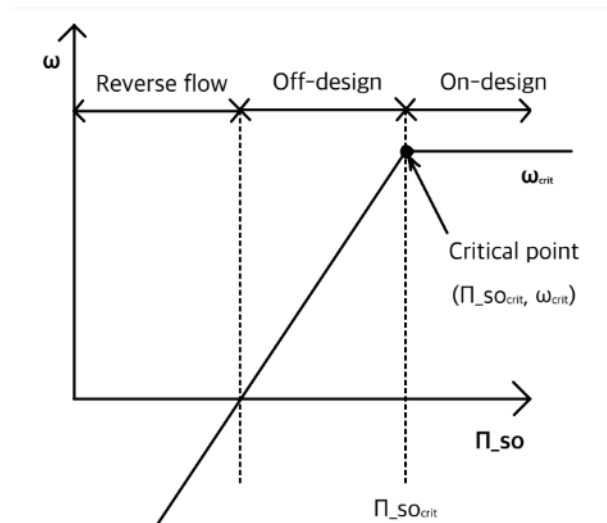

Figure 4.0.1: This project's two-dimensional plot for the operating regimes of an ejector

4.1   Setting of the simulation

In order to obtain all the different cases at study, the base parameters of the study must be varied, so as to obtain an adequate range. The variation of each one of these parameter was performed as follows:

Parameter	Increment	Range
p_p	2	[25-45] [bar]
p_s	2	[0.5-14] [bar]
Efficiency of the primary flow through the nozzle	0.05	[0.85-0.95]
Efficiency of the secondary flow suction	0.05	[0.8-0.9]
Efficiency for primary flow expansion	0.05	[0.8-0.9]
Efficiency for the mixing process	0.05	[0.8-0.9]

Table 4.1.1: Ranges of change for the variation of the parameters at study

Additionally, these changes were performed for the three different gas models at study, defined in the upper sections.

4.2   Analysis of procedure followed for analysis

With the data obtained, the pressure ratios and entrainment ratios were calculated, which were used to plot the performance map of the ejector for each case. However, considering the fact that the differences between cases are small, it cannot be easily seen the differences just by looking at the 3D map, so with the purpose of better observing the changes, the analysis was performed making "cuts" to the graphs, at three different values of the primary pressure ratios of:

Π_{po}	0.440
Π_{po}	0.333
Π_{po}	0.268

Table 4.2.1: Primary pressure ratios at study

The simplest case to analyse, the perfect gas model, will be analysed in detail. Then, seeing that the results and tendencies obtained are the same, what will be studied is the difference in the amount of variation that each gas model generates in the solution, but without discussing in detail the tendencies of each model, seeing they are the same as for the perfect gas

4.3   Analysis of the base case performance map

Knowing the expected tendencies, as shown in Section 2, it can be seen if the performance maps that are generated with the data obtained from the matlab model are accurate or not. The parameters that are displayed on the three axis of the performance plots are:

- Entrainment ratio, ω:

$$\omega = \frac{\dot{m}_S}{\dot{m}_P} \tag{6}$$

- Primary pressure ratio, Π_{po}:

$$\Pi_{po} = \frac{p_{outlet}}{p_P} \tag{7}$$

- Secondary pressure ratio, Π_{so}:

$$\Pi_{so} = \frac{p_S}{p_{outlet}} \tag{8}$$

The base cases for the three differnet gas models are going to be displayed and compared. As for the rest of the plots, they can be found in Appendix A.
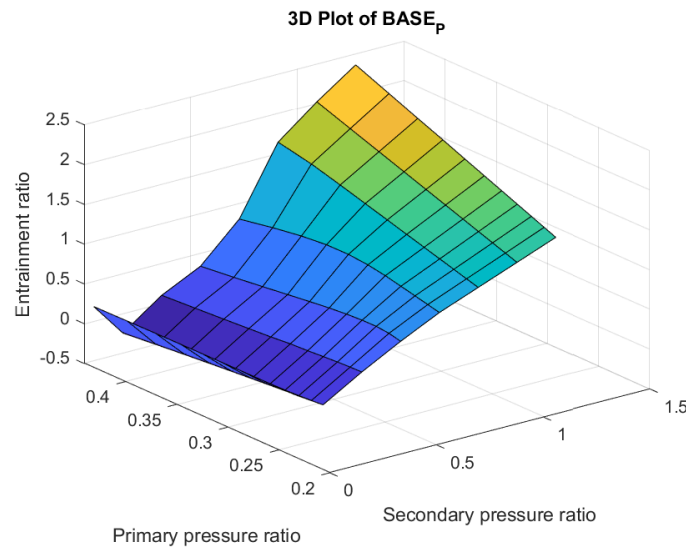
- Perfect gas model:

Figure 4.3.1: Performance map for the base case utilising perfect gas model

What can be observed in this plot is that the tendency is coincident with the expected one, except for the fact that, as the primary pressure ratio increases, the maximum entrainment ratio seen decreases. Analysing the secondary pressure ratio, it can be seen that, when decreasing the ratio, it also causes a decrease in the entrainment ratio, crossing to negative values when it has a value of approximately 0.3. Then, the ejector is in reverse flow mode. In this region, when the secondary pressure ratio goes to a value below $\Pi_{SO} = 0.18$ there

is a sudden increase in the entrainment ratio, which should not be. This is where the decrease in the accuracy of the model can be observed.
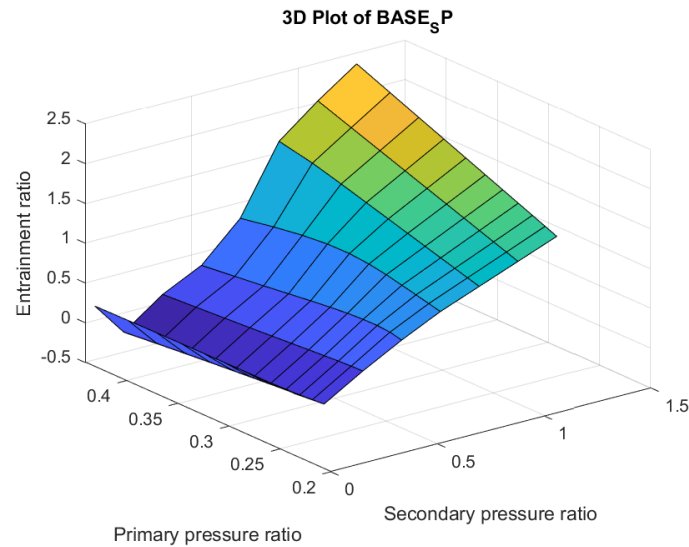
- Semi perfect gas model:

Figure 4.3.2: Performance map for the base case utilising semi perfect gas model

In this case, the behaviour observed is mostly coincident with the perfect model gas case, with the slight difference that the increase in the entrainment ratio with the secondary pressure ratio is slightly less pronounced, as well as the decrease of the entrainment ratio with the increase of the primary pressure ratio. The same errors as in the perfect case, when operating in reverse flow conditions, is observed.
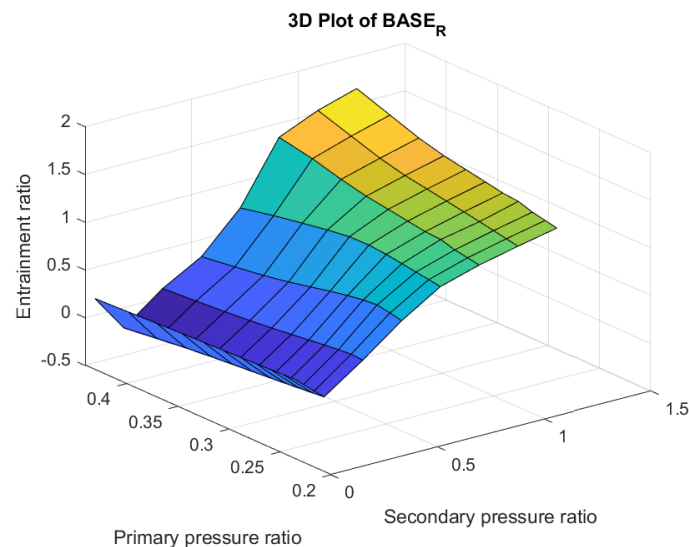
- Real gas model:

Figure 4.3.3: Performance map for the base case utilising real gas model

Last but not least, the real gas model also presents the same general behaviour as the perfect gas model. However, it can be seen that the entrainment ratio reaches maximum value of around 2, which is 20% lower than the one reached by the perfect or semi-perfect gas models. Not only that, but also the performance map has a smoother surface, meaning that the real gas model has more similar results for different pressure ratios, which is understandable when considering the fact that this gas model has properties that do not only depend on the temperature of the fluid, but also its pressure. Last but not least, in the area where the model displays inaccuracies, it can be seen that these inaccuracies have a higher value in absolute value. This means that the real gas model is more sensitive to the modelling problems and limitations.

4.4   Analysis of efficiency effect: Perfect gas

The two dimensional plot for the perfect case is displayed in the following images. In one of them, all the pressure ratios studied are displayed, while in the other one only the pressure ratios at study are displayed.
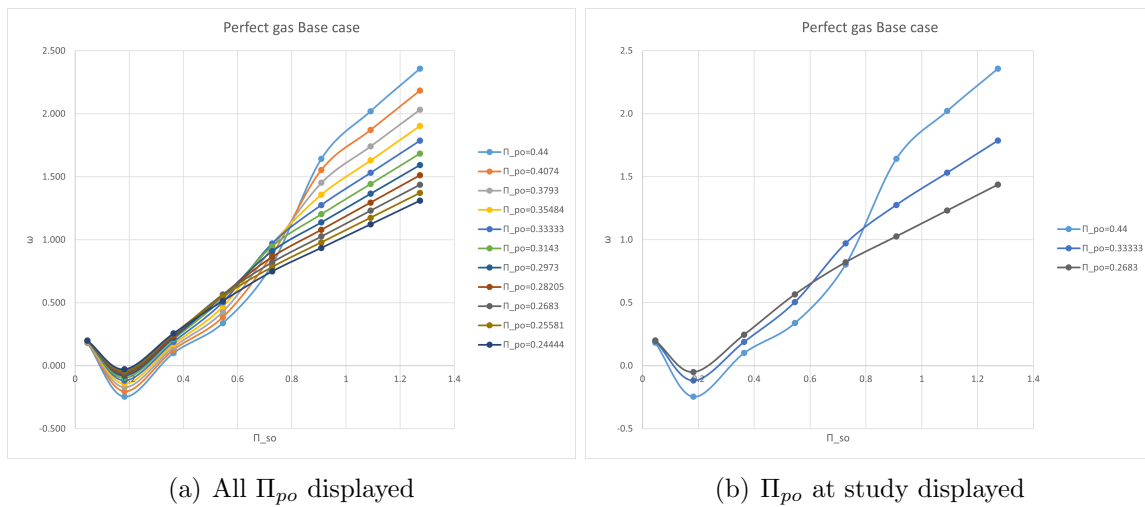

(a) All Π_{po} displayed   (b) Π_{po} at study displayed

Figure 4.4.1: Perfect gas base case two-dimensional plots

The tendency observed it the expected one: an increase in the entrainment ratio with the increase of the secondary pressure ratio, with a higher slope in the cases with higher primary pressure ratio. Also, anomalies are observed when the secondary pressure ratio is very low, when there is reverse flow. When the primary pressure ratio is low, the difference between minimum entrainment ratio and maximum entrainment ratio is also lower, compared to the case when the primary pressure ratio is the highest.

It should also be expected an area in the plot with constant entrainment ratio, when the ejector operates in critical conditions. However, considering the ranges of pressure in the simulation, this regime was never reached.

4.4.1   Effect of secondary flow suction efficiency

The two-dimensional plots corresponding to the effect that the secondary flow suction (SS) efficiency has on the entrainment ratio are displayed in the following graphs:

(a) $\Pi_{po} = 0.44$

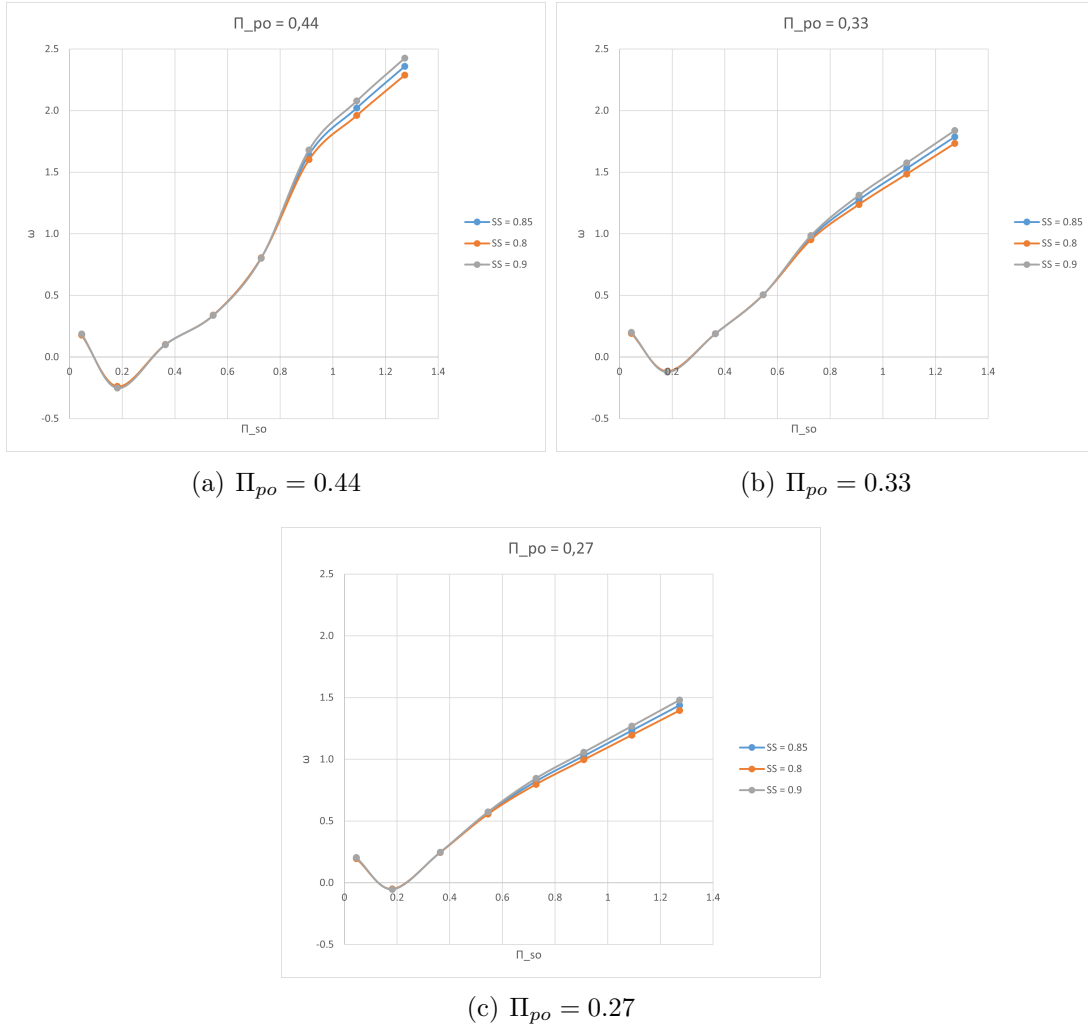(b) $\Pi_{po} = 0.33$

(c) $\Pi_{po} = 0.27$

Figure 4.4.2: Effect of η_{SS}

The efficiency of the secondary flow suction has a direct effect on the mass flow of the secondary flow into the ejector. By observing the graphs, it is seen that, regardless of the primary pressure ratio at study, the effect it has is that the increase in the value of the efficiency poses an increase in the entrainment ratio, while the opposite occurs if the efficiency decreases.

This is due to the fact, when increasing the efficiency, it means that there are less losses at the inlet of the secondary flow, due to friction with the walls or the not ideal inlet conditions, meaning that the real secondary mass flow is higher and thus closer to the ideal one. The increase in this parameter, while maintaining the primary mass flow constant, causes an increase in the entrainment ratio, considering that these two are directly proportional, as shown in Eq. (6).

It can be seen that the entrainment ratios are the same in all of the cases, until a point is reached in which they start to separate. This separation occurs at higher values of the secondary pressure ratio if the primary pressure ratio is also high because, in this situation, the pressure of the secondary flow increases and thus increases the secondary mass flow with respect to the primary flow, making more relevant the effects of the suction of the secondary flow. Another possible explanation is that, in the mathematical equations that define the entrainment ratio when the flow is chocked, it is given mode importance to this efficiency.

Additionally, the variation it causes in both cases is virtually the same, and is virtually constant also for the different values of the primary pressure ratio choice. These variations are displayed in the subsequent table:

η_{SS}	$\Pi_{po} = 0.440$	$\Pi_{po} = 0.333$	$\Pi_{po} = 0.268$
0.8	-2.99%	-2.98%	-2.98%
0.9	2.90%	2.90%	2.90%

Table 4.4.1: Percentage of variation of entrainment ratio when varying the secondary flow suction efficiency measured at $\Pi_{so} = 1.09$

4.4.2   Effect of primary flow through nozzle efficiency

The two-dimensional plots corresponding to the effect that the primary flow through nozzle efficiency (PN) has on the entrainment ratio are displayed in the following graphs:

(a) $\Pi_{po} = 0.44$

(b) $\Pi_{po} = 0.33$

(c) $\Pi_{po} = 0.27$
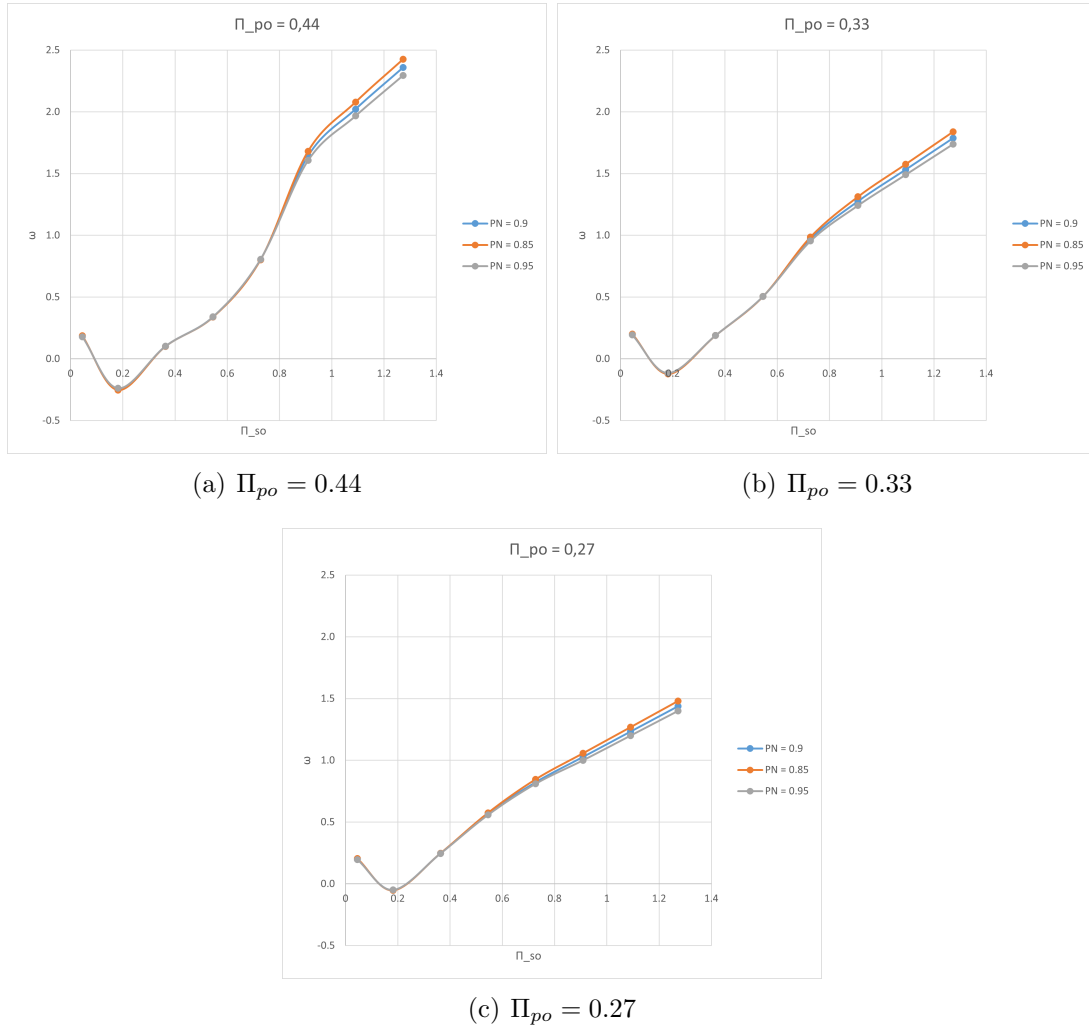
Figure 4.4.3: Effect of η_{PN}

The efficiency of the primary mass flow through the nozzle has a direct effect on the primary mass flow into the ejector. It accounts for the losses of this flow when passing though the nozzle, due to phenomena like friction. In this case, the observed behaviour is the opposite than the one in the previous case: the increase in the efficiency poses a decrease in the entrainment ratio, and vice versa.

When increasing the efficiency, that means that less primary mass flow is lost at the inlet, so the real value is closer to the ideal one. Considering that for all the cases the secondary mass flow has remained constant, and seeing in the expression displayed in Eq. (6) that the relationship between the primary mass flow and the entrainment ratio is inversely proportional, this behaviour can be understood.

As in the previous case, the entrainment ratios coincide, until there is a point in which they start to diverge. This divergence occurs at higher values of the secondary pressure ratio if the primary pressure ratio is also high for similar reasons as in the previous case, which is that at these values of the secondary mass flow, its effects are more relevant than the ones of the

primary mass flow.

As in the previous case, the difference that the choice of efficiency causes in the entrainment ratio is basically the same regardless of the primary pressure ratio chosen, but slightly lower with respect to the previous efficiency.

η_{PN}	$\Pi_{po} = 0.440$	$\Pi_{po} = 0.333$	$\Pi_{po} = 0.268$
0.8	2.89%	2.89%	2.89%
0.9	-2.67%	-2.67%	-2.67%

Table 4.4.2: Percentage of variation of entrainment ratio when varying the primary flow through nozzle efficiency measured at $\Pi_{so} = 1.09$

4.4.3   Effect of primary flow expansion efficiency

The two-dimensional plots corresponding to the effect that the primary flow expansion efficiency (PE) has on the entrainment ratio are displayed in the following graphs:

(a) $\Pi_{po} = 0.44$
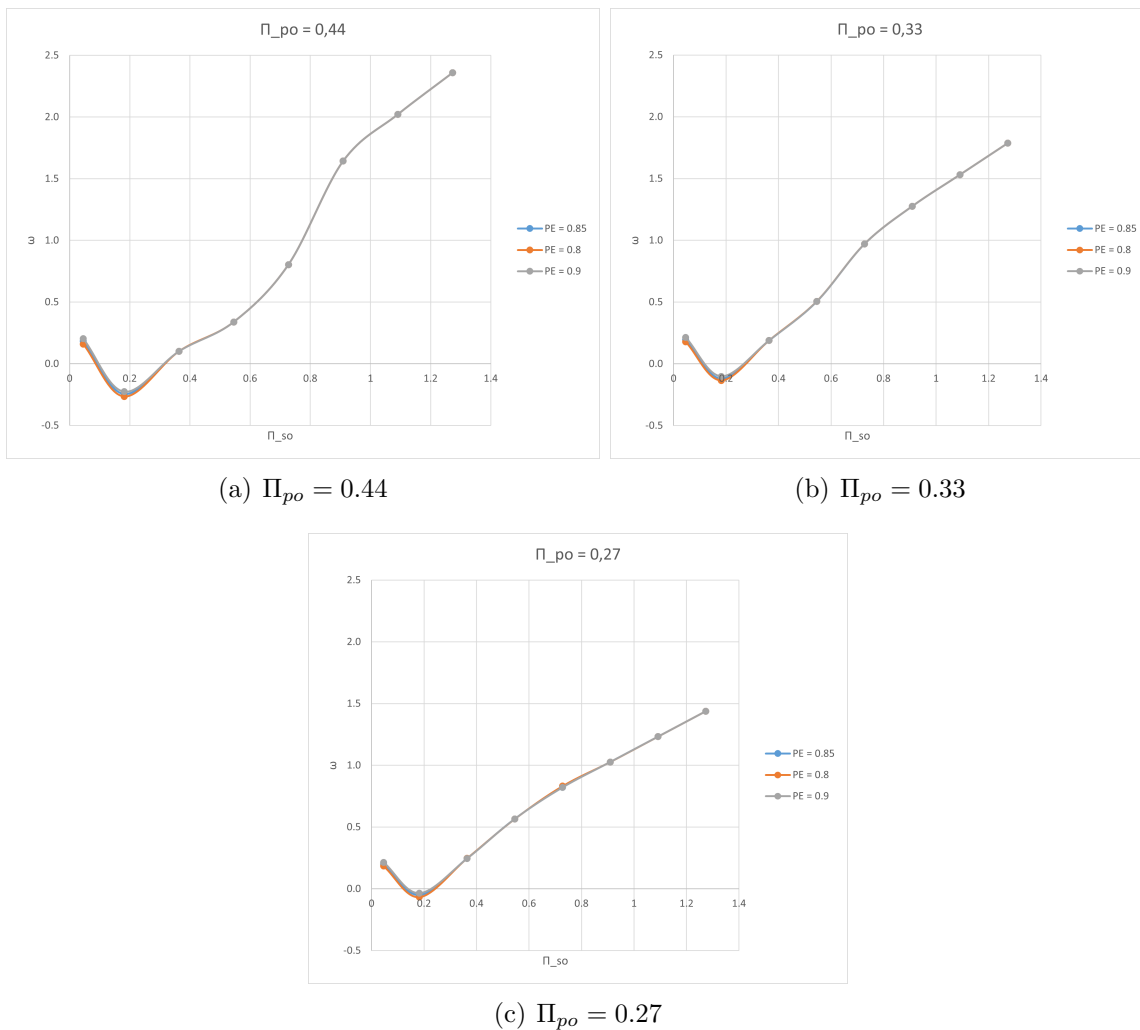

(b) $\Pi_{po} = 0.33$

(c) $\Pi_{po} = 0.27$

Figure 4.4.4: Effect of η_{PE}

The efficiency of the primary flow expansion has a direct effect on the effective area of expansion of the primary flow when exiting the nozzle. Its increase causes the area to be bigger, and thus closer to the ideal one, while the decrease of the same has the opposite effect. This increase in efficiency efficiency may be considered beneficial, but it must be remembered that if the primary flow expansion area is higher, it leaves less area for suction of the secondary flow. Likewise, the decrease in efficiency may not be negative, for it allows more secondary flow in the ejector, possibly increasing the entrainment ratio.

Despite these hypotheses and explanations, it is actually observed that the variation of this efficiency causes no effect on the entrainment ratio, which is maintained the same in all the cases.

The only case where presents some deviations is when operating in reverse flow conditions. This can be explained considering the model limitations when modeling this regime, because when considering isentropic flow with efficiencies and that only models one normal shock wave, which is placed in the mixing channel. The rest of the shock-waves that are generated in this regime are not modeled.

Furthermore, in this case, this efficiency does not affect the entrainment ratio, like the previous ones, because it is not related to the mass flow, but rather to the velocity of the mixed fluid. Thus, this efficiency is only observed when operating in sub-critical mode, and not in the critical one, when both flows are blocked.

The variations observed in this case are displayed in the following table. It must be noted that, even though the percentages are of extremely high value, it must be reminded that the values with which it is dealt are extremely low, so this variation in reality is neglegible.

The reduction in the primary pressure ratio generated a higher variation in the entrainment ratio, but the variation caused by the choice of efficiency is the same for both the increase and the decrease of it.

η_{PE}	$\Pi_{po} = 0.440$	$\Pi_{po} = 0.333$	$\Pi_{po} = 0.268$
0.85	7.92%	14.15%	29.87%
0.95	-7.92%	-14.21%	-30.28%

Table 4.4.3: Percentage of variation of entrainment ratio when varying the primary flow expansion efficiency measured at $\Pi_{so} = 0.18$

4.4.4   Effect of mixing efficiency

The two-dimensional plots corresponding to the effect that the mixing efficiency (M) has on the entrainment ratio are displayed in the following graphs:

(a) $\Pi_{po} = 0.44$

(b) $\Pi_{po} = 0.33$

(c) $\Pi_{po} = 0.27$
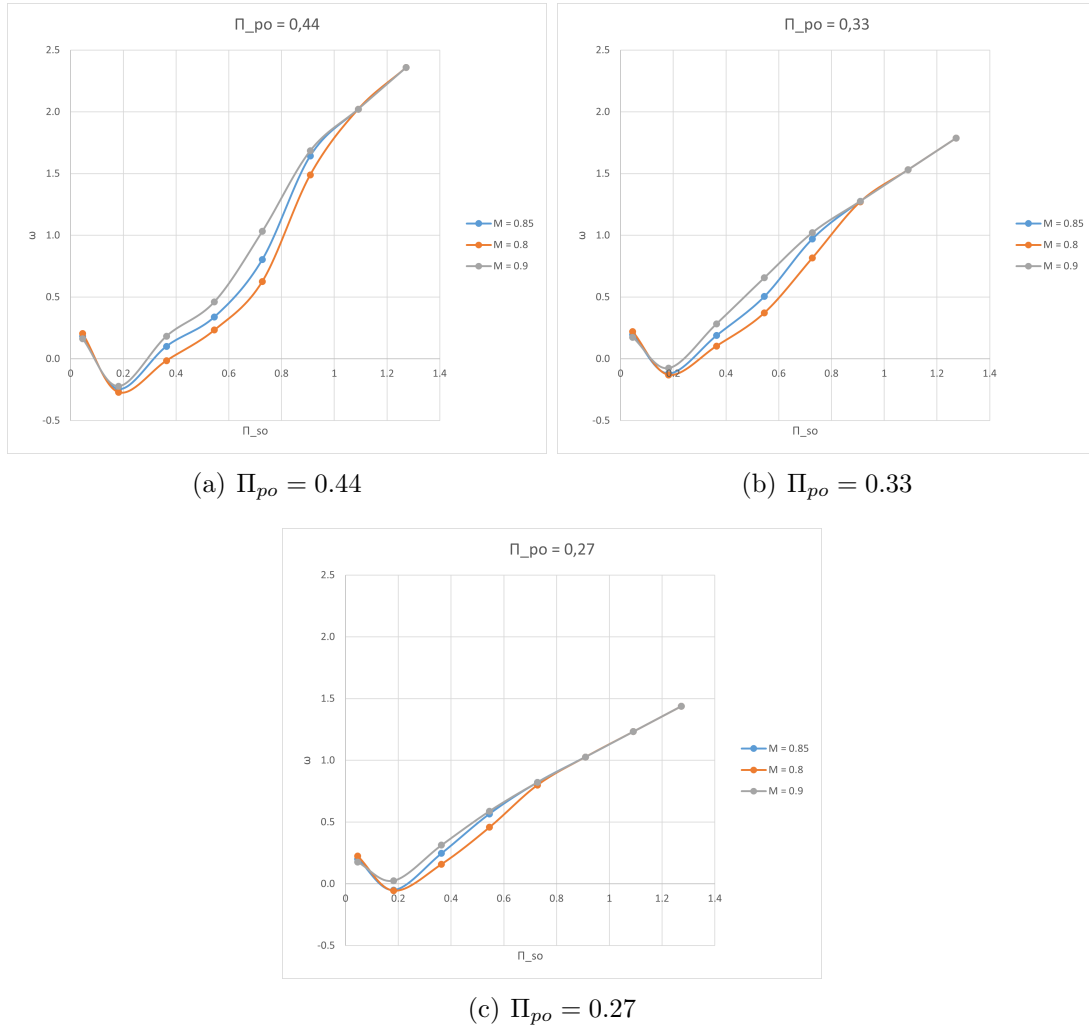
Figure 4.4.5: Effect of η_M

The mixing efficiency has a direct effect on the velocity of the mixed fluid. A higher value of the same implies a more uniform, homogeneous and faster mix, giving as a result a fluid that is closer in properties to the ideally calculated one. The increase in the efficiency causes an increase in the entrainment ratio, and the opposite in the case of decreasing efficiency, This is because when the efficiency increases, the kinetic energy that the high-pressure and high-velocity primary flow has is more effectively transferred to the secondary flow, causing the mix to have increased momentum and velocity. This allows for the suction of more secondary mass flow, which is directly proportional to the entrainment ratio.

It can be seen that the tendencies of the entrainment ratio are convergent, arriving a moment when the curves for the three different efficiencies coincide. The moment when this overlap occurs, is at higher secondary pressure ratios the higher the primary pressure ratio is, and the opposite in the case when the primary pressure has a lower value.

The maximum variation occurs when $\Pi_{so} = 0.54$, and the values are displayed in the following table. It can be seen that the variation caused by the decrease of the efficiency

is higher in absolute value than the caused by the increase of the efficiency. Additionally, the decrease of the primary pressure ratio causes a decrease in this variation. At the lowest pressure ratio analysed, the difference between the trends is the highest.

This is because, just like in the previous case, this efficiency does not affect the entrainment ratio, like the previous ones, because it is not related to the mass flow, but rather to the velocity of the mixed fluid. Thus, this efficiency is only observed when operating in sub-critical mode, and not in the critical one, when both flows are blocked.

η_M	$\Pi_{po} = 0.440$	$\Pi_{po} = 0.333$	$\Pi_{po} = 0.268$
0.8	-31.29%	-26.31%	-19.23%
0.9	36.14%	29.96%	3.95%

Table 4.4.4: Percentage of variation of entrainment ratio when varying the mixing efficiency measured at $\Pi_{so} = 0.54$

However, it can be seen that the curves also overlap for very low values of the secondary pressure ratio. This can be considered anomalous behaviour, and can be explained considering the model limitations when the ejector operated in reverse flow conditions. The variations caused are displayed in the following table, and it can be seen that for the lower efficiency the variation is maintained almost constant in all the cases. However, when the efficiency is increased, there is also an increase in the variation, in absolute value.

η_M	$\Pi_{po} = 0.440$	$\Pi_{po} = 0.333$	$\Pi_{po} = 0.268$
0.8	10.48%	10.19%	10.14%
0.9	-9.60%	-35.32%	-149.21%

Table 4.4.5: Percentage of variation of entrainment ratio when varying the mixing efficiency measured at $\Pi_{so} = 0.18$

4.5   Analysis of efficiency effect: Semi-perfect gas

To begin with the comparison of the semi-perfect gas to the real one, the graphs that represent its basic case are going to be displayed in Fig. 4.5.1.

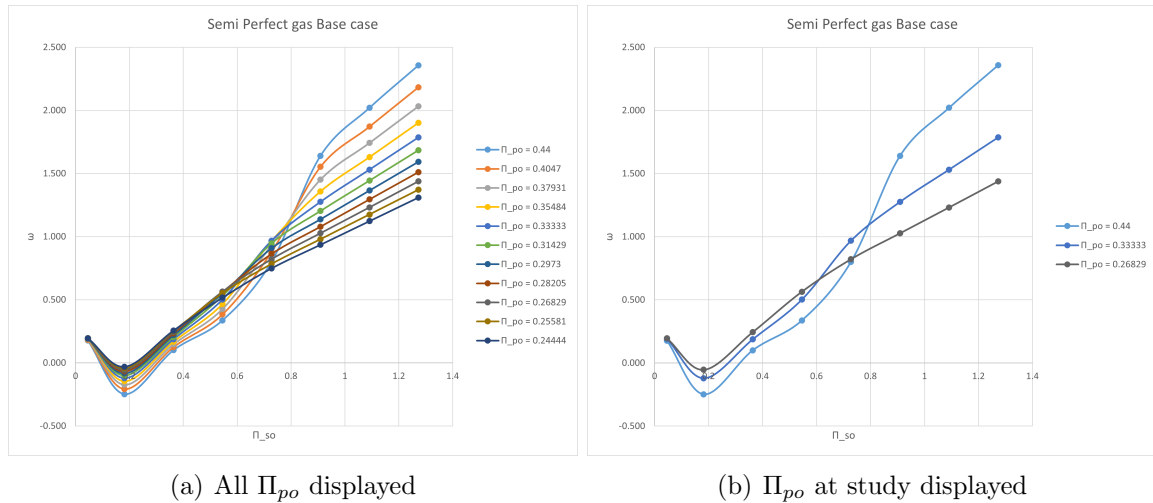(a) All Π_{po} displayed

(b) Π_{po} at study displayed

Figure 4.5.1: Semi perfect gas base case two-dimensional plots

When comparing to the perfect case, no major difference can be observed in the tendencies. The behaviour of the entrainment ratio is maintained, and the gas model choice does not evidently influence the behaviour.

All the rest of the graphs for each efficiency are displayed in the annex, for the tendencies are also the same, but only with different variation percentages.

4.5.1   Effect of secondary flow suction efficiency

As it can be seen in the table displayed below, the variation that the efficiency change causes is virtually the same for both gas models, which implies the same consequences as in the perfect gas model case.

The increase in the efficiency causes an increase in the entrainment ratio, because it implies that there are less losses in the entry of the secondary flow inlet.
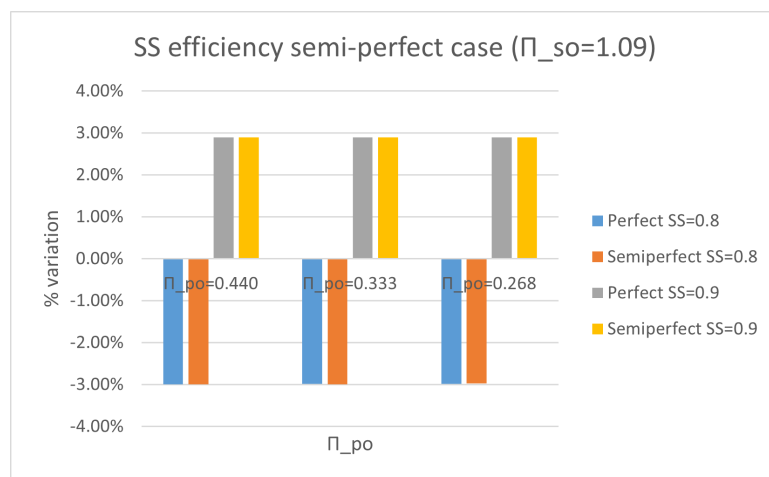
Figure 4.5.2: Effect of secondary flow efficiency measured at $\Pi_{so} = 1.09$

4.5.2   Effect of primary flow through nozzle efficiency

Comparing the effect of the primary flow through nozzle efficiency for the perfect and semi perfect gas models, as in the previous case, it can be seen that the variations it causes are virtually the same. The slight difference resides that the semi perfect variations are different for the different pressure ratios, whereas in the perfect gas model case the differences are maintained constant.

Just as in the perfect gas model case, the increase of this efficiency implies a reduction in the entrainment ratio, due to the fact that more primary mass flow enters the ejector.
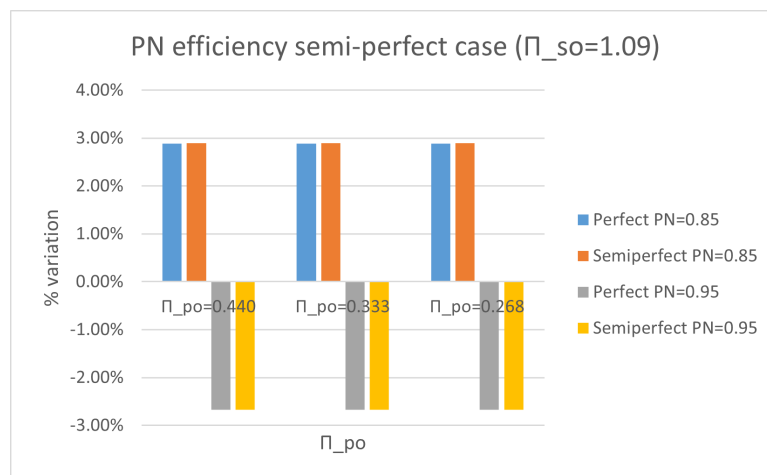
Figure 4.5.3: Effect of primary flow through nozzle efficiency measured at $\Pi_{so} = 1.09$

4.5.3   Effect of primary flow expansion

It can be observed that the increasing variation in the entrainment ratio with the reduction of the primary pressure ratio is conserved, while also observing that the choice of a semi perfect gas makes the difference slightly lower in each case. These differences are observed for low secondary pressure ratios, where there is reverse flow conditions. In the single choking operation mode, there is no variation between the entrainment ratios.

Like in the perfect gas model case, this efficiency has no effect in the entrainment ratio, except in the reverse flow mode.
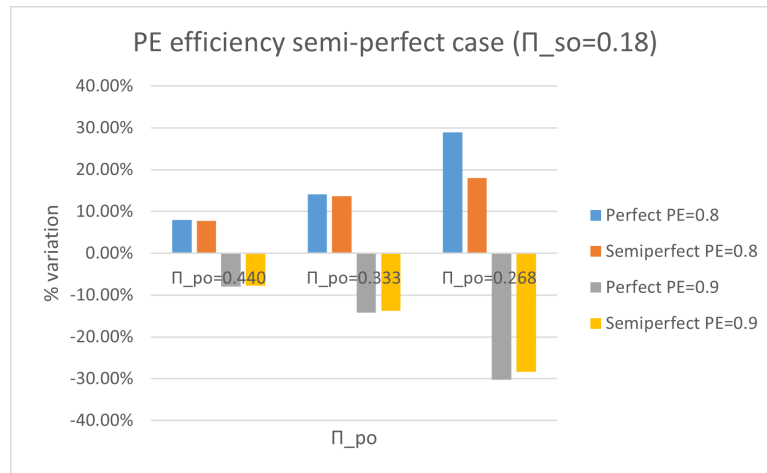
Figure 4.5.4: Effect of primary flow expansion efficiency measured at $\Pi_{so} = 0.18$

4.5.4   Effect of mixing efficiency

The general behaviour for this gas model is the same as the one in the perfect gas model case, both in the expected behaviour and the anomalies in the reverse flow operation.

In the expected behaviour it can be seen that also the divergence occurs at lower secondary pressure ratios as the primary pressure ratio decreases. The maximum variations, which occur at $\Pi_{so} = 0.54$ are displayed in the following table. Generally, the variations in the semi perfect gas model are slightly lower.
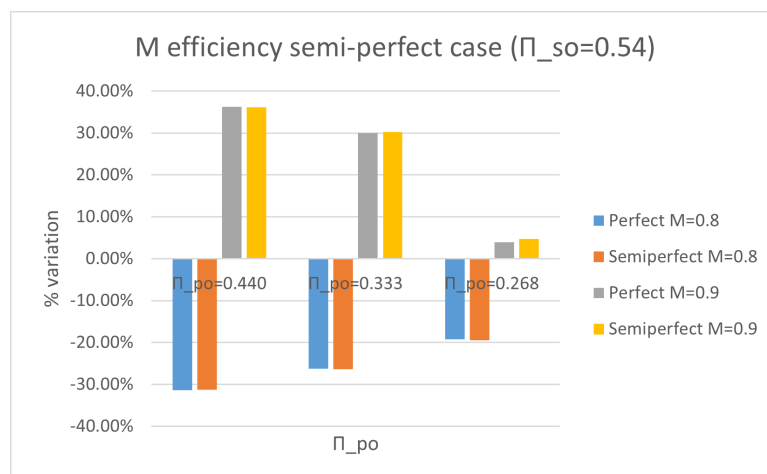
Figure 4.5.5: Effect of mixing efficiency measured at $\Pi_{so} = 0.54$

In the region with abnormal behaviour, it can be observed the same tendencies in the variation as for the perfect gas model. The choice of the semi perfect gas model causes a slight increase in the variation in this area.
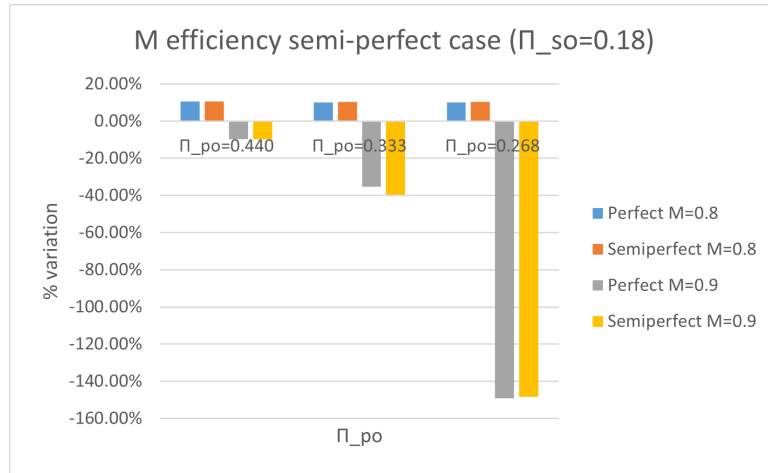
Figure 4.5.6: Effect of mixing efficiency measured at $\Pi_{so} = 0.18$

4.6   Analysis of efficiency effect: Real gas

To begin with the comparison of the semi-perfect gas to the real one, the graphs that represent its basic case are going to be displayed in Fig. 4.6.1.
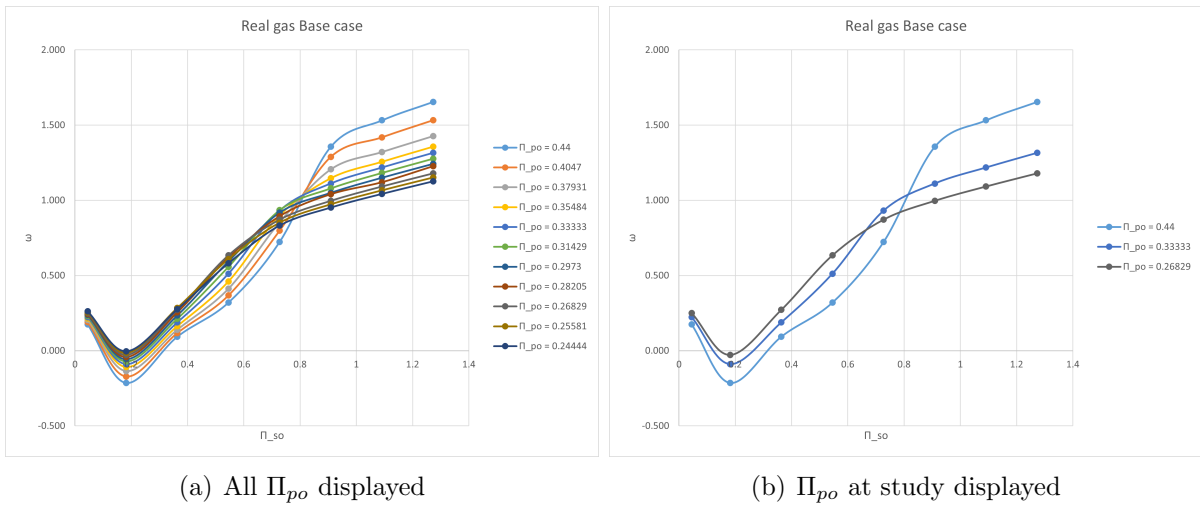

(a) All Π_{po} displayed

(b) Π_{po} at study displayed

Figure 4.6.1: Semi perfect gas base case two-dimensional plots

When comparing to the perfect case, no major difference can be observed in the tendencies. The behaviour of the entrainment ratio is maintained, and the gas model choice does not evidently influence the behaviour. The only variation observed is a general decrease in the entrainment ratio, to values of under 2, while in the perfect gas model it reached values of almost 2,5. This can be explained considering the losses and limitations that the real gases have.

All the rest of the graphs for each efficiency are displayed in the annex, for the tendencies are also the same, but only with different variation percentages.

4.6.1   Effect of secondary flow suction efficiency

The choice of a real gas model has the same effect that the choice of a semi perfect gas model: none. The variations are maintained the same for all pressure ratios. The only difference is the decrease in absolute value of the entrianment ratio, but the variation of efficiencies causes the same effect as for the other gas models.
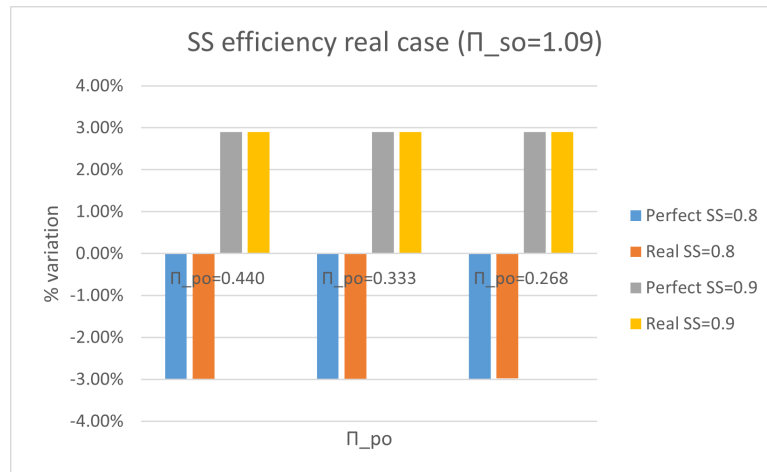

Figure 4.6.2: Effect of secondary flow suction efficiency measured at $\Pi_{so} = 1.09$

4.6.2   Effect of primary flow through nozzle efficiency

Like for the previous efficiency, the choice of model does not cause a change in the variations that the choice of efficiency causes. The only difference would be the absolute value of the entrainment ratio for each case, where the real model has a lower value than the perfect one.
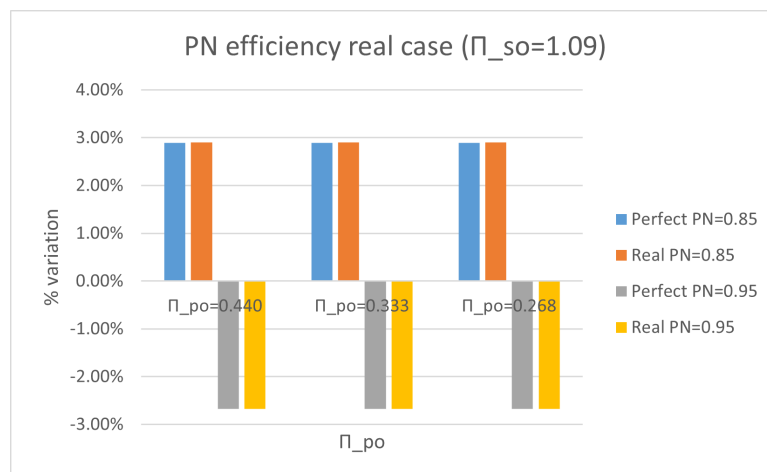

Figure 4.6.3: Effect of primary flow through nozzle efficiency measured at $\Pi_{so} = 1.09$

4.6.3   Effect of primary flow expansion

In this case, the choice of the real gas model has a more significant effect in the variation, increasing the percentage for every pressure ratio. This did not happen for the semi perfect model. As a consequence, it can be said that choosing the real model would cause more sensitivity of the simulation to the choice of one value of the primary flow expansion or other, while choosing a model that is perfect or semi perfect would not cause such a disturbance.
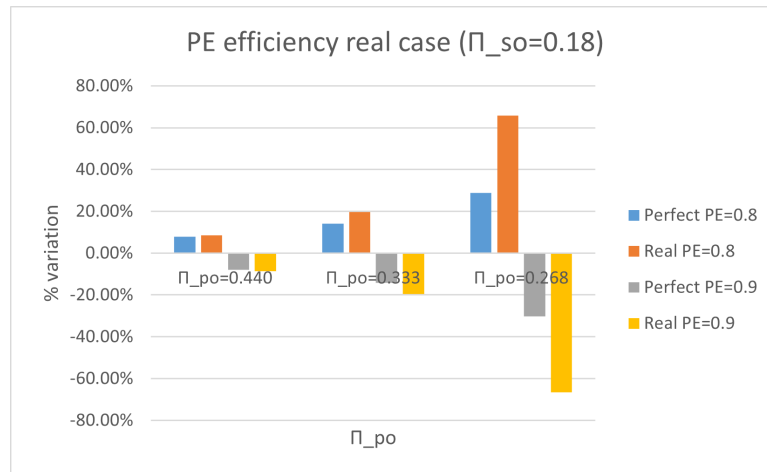

Figure 4.6.4: Effect of primary flow expansion efficiency measured at $\Pi_{so} = 1.09$

4.6.4   Effect of mixing efficiency

The general behaviour for this gas model is the same as the one in the perfect gas model case, both in the expected behaviour and the anomalies in the reverse flow operation.

The difference resides that in this case the variations caused by the choice of the real model, in the normal behaviour region, are less than then ones caused by the other model. This makes the real gas model more resistant to efficiency choice.
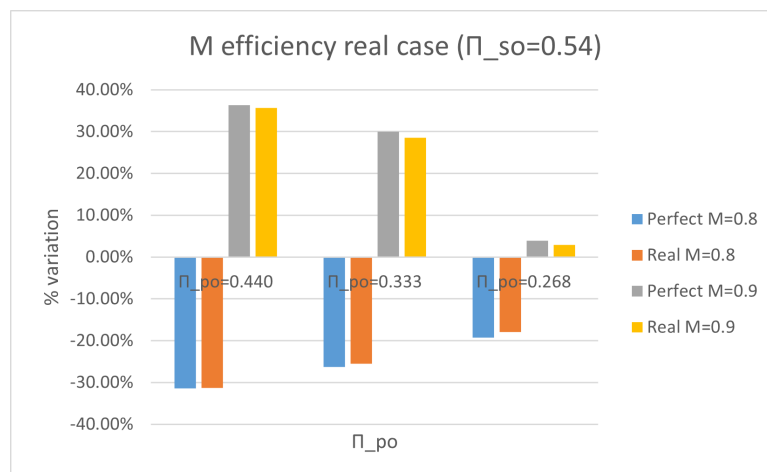

Figure 4.6.5: Effect of mixing efficiency measured at $\Pi_{so} = 0.54$

In the region with abnormal behaviour, it can be observed the same tendencies in the variation as for the perfect gas model. The choice of the real gas model causes a decrease in the variation as well.
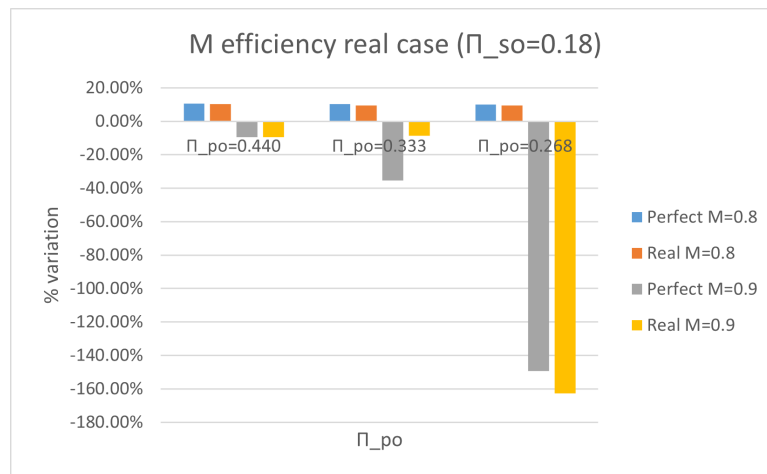

Figure 4.6.6: Effect of mixing efficiency measured at $\Pi_{so} = 0.18$

5   Conclusions

To properly summarize and order the final conclusions obtained in this study, this section is written. It is structured in two subsections, each one of them corresponding to one of the questions that initiated and drove this project from the beginning, and where the culmination of all the results can be found in the form of a summary.

5.1   Accuracy of model when working in reverse flow conditions

The comparison between the theoretical performance map of an ejector and the ones obtained from the simescape model simulations, yields to the following conclusion: the model does, in fact, not provide accurate nor realistic results when operating in reverse flow conditions.

In theory, when the ejector enters the reverse flow mode, the entrainment ratio should be constantly decreasing. However, when plotting the performance maps obtained with the data from the simulations, it can be observed that this tendency is not maintained.

When the Π_{so} reaches a value of approximately 0.2, and for values below this aforementioned one, the graph shifts and starts to increase, rather than continuing the decreasing tendency expected and theoretically endorsed.

This is explained when taking into account the numerous simplifications and assumptions that the model presents, among which the fact that the flow is considered isentropic is found. This isentropic flow considers some efficiencies, in order to make the results closer to the real ones. Additionally, if necessary, it will model one normal shockwave and place it in the mixing channel. This greatly simplifies the calculations, but is not very accurate when there are more shockwaves generated. These can be generated when the ejector is working in sub-critical mode or reverse flow mode. Not modelling them is observed to cause divergence in the expected and obtained results.

5.2   Effect of efficiencies variation over performance

The choice of value of an efficiency describing a process or another is of high importance. Nevertheless, it is not the only factor that ultimately affects the obtained results, for the effect of each efficiency can be attenuated or aggravated by the choice of gas model.

- Effect of the secondary flow efficiency (SS).

    The increase of this efficiency leads to an increase of the entrainment ratio, because it implies that there are less losses at the inlet of the secondary flow port. If the primary mass flow is kept constant, then the increase in the secondary mass flow into the ejector implies an increase in the entraimnent ratio.

In this case, the choice of the gas model is not relevant, since the variation caused in the results upon the change of the efficiency value is the same in all of the cases.

- Effect of the primary flow through the nozzle efficiency (PN).

The increase of this efficiency has the opposite effect than the previous one: it leads to a decrease of the entrainment ratio, because it implies that there are less losses at the inlet of the primary flow port. If the secondary mass flow is kept constant, then the increase in the primary mass flow into the ejector implies an decrease in the entraimnent ratio, considering they are inversely proportional.

In this case, the choice of the gas model is not relevant, since the variation caused in the results upon the change of the efficiency value is the same in all of the cases.

- Effect of the primary flow expansion efficiency (PE).

In the case when this efficiency is varied, there is no effect in the entrainment ratio. This is due to the fact that this efficiency does not affect the mass flow rate of the primary nor secondary ratio, but rather the expansion of the primary flow. The only situation in which an actual effect can be observed is when operating in reverse flow conditions, but this can be explained considering the model limitations and assumptions. In this case, the variations that are compared are for the secondary pressure ratio at which the change in tendency occurs. Despite the fact that the difference in values is percentagely high, it must be remembered that the values dealt with are very low, so the variation in absolute value is not so considerable.

In this case, the choice of gas model has an influence on the entrainment ratio, since choosing a real gas model causes higher variation when changing the efficiency, whereas a semi-perfect gas model is not so sensitive to primary flow expansion mixing efficiency variation.

- Effect of the mixing efficiency (M).

The mixing efficiency has an effect on the velocity of the mixed fluid. Increasing its value causes an increase in the entrainment ratio, and the opposite in the opposite case. The tendency is convergent, meaning that for a higher value of the secondary pressure ratio, the entrainment ratios for the different efficiencies converge. This convergence occurs for lower values of the secondary pressure ratio when the primary pressure ratio also has a low value, which is explained considering the fact that, for these values, both fluids have the same influence and effect. There is an anomaly when the model operated in reverse

flow, at a value of the secondary pressure ratio of around 0.2, where when decreasing
this pressure ratio causes a convergence. Again, these results are not accurate due to the
limitations and assumptions that the model makes.

In this case, the choice of gas model has an influence on the entrainment ratio. Opposite
as in the previous case, the real gas model causes less variation when changing the value
of the efficiency, while the semi-perfect gas model is more sensitive.

5.3   Final remarks

Therefore, generally, the choice of the gas model does not affect the results obtained, except
for the fact that the real gas model is more resistant to variations of the mixing efficiency,
and the semi-perfect gas model is more resistant to changes in the primary flow expansion
efficiency. However, in all cases, these variations are not very high, therefore choosing a perfect
gas model is ideal, since it reduces computational time and cost without highly compromising
the accuracy of the results. Furthermore, the choice of a value of the efficiency or another does
not significantly affect the results obtained, therefore it can be concluded that the model is
resistant enough for all the different gas models.

Nevertheless, all of these conclusions do not apply to the reverse flow mode of operation,
where unrealistic phenomena, like the increase of the entrainment ratio when the secondary
pressure ratio has a value below approximately 0.2 occurs. Additionally, in this region, the
variation of the efficiencies has a higher effect. For that reason, it is advisable to avoid this
operational region.

6 Budget

This section's purpose is the breakdown and disclosure of the cost that this project involves. The resources utilised for the development of this paper consist of technological resources, both hardware and software, as well as the labor of the student in the research, processing and analysis of the data. All this process has been supervised by the thesis director. Despite the fact that the author of this thesis is a student, and therefore has some privileges obtaining licenses for free (due to educational agreements between the university and the institutions in charge of developing and managing the software licenses), the cost breakdown will not consider this. It will, in fact, asses the costs that would be given the author is an engineer, and that there are no educational privileges.

6.1 Technological resources

These resources can be divided in two sections: the hardware and the software. Hardware comprises all physical elements that compose the computer, and through which the user inputs the data that the software will process, and will later display. Software, on the other hand, is the set of programs, data or instructions that computers require to operate and complete certain tasks.

6.1.1 Hardware

A summary of what the items employed and their individual costs is presented in Table 6.1.1.

Hardware	
Item	**Cost [€]**
Computer	64
Mouse	10
Tablet	650
TOTAL	724

Table 6.1.1: Hardware cost breakdown

In detail:

- Computer: which was used to run the different Matlab cases, as well as storing the data in Excel for later processing, which included generating the 3D plots and the 2D graphs, on which analysis was performed and conclusions were obtained. The model of the computer employed is *HP 15s-fq1158ns*, with:

  – Processor: Intel(R) Core(TM) i7-1065G7 CPU @ 1.30GHz 1.50 GHz.

  – Installed RAM: 16 GB (15.7 GB usable).

– SSD/HDD: 512 GB.

The cost of the computer can be broken down into:

$$Cost = Original price \cdot \frac{Months of usage}{Monts of life time} = 800 \cdot \frac{4}{50} = 64$$

- Mouse: which was used to facilitate and accelerate the handling of the programs and analysis. The model of the mouse used is *Logitech M90.*

- Tablet: which was used to perform the research, by allowing to better handle the papers, as well as structuring the analysis of the results. The model employed is *Ipad Air 4th generation.*

6.1.2   Software

The breakdown of cost of the programs utilised is performed in Table 6.1.2. It is important to mention that these licenses were provided by the university, for free, due to the educational agreements in place. However, these costs are the hypothetical cost that would take place had the author of this thesis not been a student, but rather an engineer.

Software			
Item	**Time [year]**	**Price [€/year]**	**Cost [€]**
Matlab	1	203.63	203.63
Office	1	140.74	140.74
Overleaf	-	-	0
TOTAL			344.37

Table 6.1.2: Software cost breakdown

In detail:

- Matlab: which is a software developed by Mathworks. Within it, there is the Simescape library, which is the one that was used to run the simulations of the different cases. Additionally, Matlab was used to perform the 3D plots of the performance maps of the ejector.

- Office: which is a suite of applications created by Microsoft with the purpose of increasing productivity and completing common tasks. In this case, the applications used from the complete package were:

  – Excel: which was used to store the results of the simulation, as well as for performing the different graphs what were used to analyse the trends of the resutls and the effects of the variation of the paramters.

– Teams: which was the main communication channel between the author of this paper and the supervising and guiding professor.

• Overleaf: which was used for the composition of this present document. The basic package, available for everyone, is free of cost. If extra features are desired, they can be purchased, but in this case, the basic one provided all the necessary resources.

6.2   Human resources

In this section, the costs of what the engineer in charge of the project would be is displayed, separating into the different activities that were necessary to complete this project. A summary of these is presented in Table 6.2.1

HUMAN RESOURCES			
Item	**Time [h]**	**Price [€/h]**	**Cost [€]**
Research	20		240.4
Simulation time	41		492.82
Post-processing	15	12.02	180.3
Analysis of results	10		120.2
Redaction of memoir	125		1502.5
TOTAL	81	-	2536.22
Tutor follow-up and help	25	40	1000

Table 6.2.1: Human resources cost breakdown

In detail:

• Research: which included reading the different documents provided, as well as understanding the operation of the software and the design of the model.

• Simulation time: which consists on the time invested in imputing the different conditions, running the case and storing the results.

• Post-processing: process which consisted in storing the data, calculating the parameters necessary for the plots and performing said plots.

• Analysis of the results: in which a detailed analysis of the effects of varying the efficiency is performed, as well as the explanation of the physical phenomena that causes them.

• Redaction of the memoir: which consists of writing this present document.

It is interesting to mention that the cost per hour is of an engineer who would hypothetically be paid 25.000 brute €/year.

Last but not least, tutor followup and help consists in the time invested by the tutor in making calls, answering doubts, correcting and overseeing the advance of the project.

6.3   Total

Adding all the individuals costs displayed above:

Item	Cost [€]
Hardware	724
Software	344.37
Human resources	2356.22
Tutor work	1000
TOTAL	4364.14

Table 6.3.1: Brute total cost

To this, a 10% in industrial profit, as well as a 21% in VAT (IVA in Spanish) must be added. Therefore, the net cost of the project is:

Brute total	-	4604.59
Industrial profit	10%	460.46
IVA	21%	966.96
Net Total		**6032.01**

Table 6.3.2: Real total cost

7 Project accordance with the sustainable development goals

The Sustainable Development Goals, SDG, are *"a universal call to action to end poverty, protect the planet, and ensure that by 2030 all people enjoy peace and prosperity"* [9]. These are the displayed in the Fig. 7.0.1:

Figure 7.0.1: Sustainable Development Goals

The governments of each country try to implement legislation that are in accordance with these, as well as the industry. This project, being an engineering paper, is no different, and it must follow the guidelines that the United Nations are suggesting in order to achieve a better future.

Some of the goals are not related to this paper's purpose, for they focus on social issues, or biologically endangered ecosystems, and how to protect them. The ones that are more fit for this case are the goals that are related to the industry, which is where many ejectors can be applied in order to improve the efficiency of the processes, as well as reducing the waste generated and ultimately reducing the impact of the industrial processes on the planet, which is a growing concerning topic.

In the end, all the goals intertwine, for all of them require of the rest in order to propeperly succeed.

In order to better display with which goals this project is related, the following table was generated:

Goal	Alignment	How
1. No poverty	No	-
2. Zero hunger	No	-
3. Good health and well being	No	-
4. Quality education	No	-
5. Gender equality	No	-
6. Clean water and sanitation	No	-
7. Afforable and clean energy	Yes	
8. Decent work and economic growth	No	-
9. Industry, innovation and infrastructure	Yes	Ejectors can be the future in energy recovery systems
10. Reduced inequalities	No	-
11. Sustainable cities and communities	No	-
12. Responsible consumption and production	Yes	Recovering heat makes the cycles more efficient, producing less waste
13. Climate action	Yes	Less waste generated contibutes to the reduction of pollution generated by the industry
14. Life below water	No	-
15. Life on land	No	-
16. Peace, justice and strong institutions	No	-
17. Partnership for the goals	No	-

Table 7.0.1: SDG with which this project aligns

A   Appendix

In this section, things such as the data tables that are created but are not crucial for the understanding of the document are presented

A.1   Semi perfect gas vectors

T [K]	h $\left[\frac{kJ}{kg}\right]$	c_p $\left[\frac{kJ}{kg\cdot K}\right]$	$\mu[s \cdot u \cdot Pa]$	k $\left[\frac{mW}{K\cdot m}\right]$
150	275.2647837305	1.0121149239	10.3766056544	14.1517155766
160	285.3770541777	1.0104210553	10.9908682445	15.0474512994
170	295.4745789036	1.0091415901	11.5932000841	15.9300520513
180	305.5608710696	1.0081589827	12.1841060353	16.7998749295
190	315.6384907840	1.0073968834	12.7640677090	17.6573089963
200	325.7093737872	1.0068048457	13.3335437107	18.5027588910
250	376.0080336495	1.0055419122	16.0381490651	22.5644026699
300	426.2977847412	1.0063738992	18.5373404837	26.3844656766
350	476.6787883239	1.0092105862	20.8671495114	30.0032801169
400	527.2538906844	1.0141440444	23.0554226801	33.4532006033
450	578.1272273519	1.0211129959	25.1239717992	36.7600619429
500	629.3950408652	1.0298687892	27.0901379793	39.9446251242
550	681.1376901312	1.0400382050	28.9679074983	43.0237448740
600	733.4154428730	1.0512032004	30.7687111230	46.0112537034
650	786.2678943768	1.0629631285	32.5020036481	48.9186234516
700	839.7158511520	1.0749711171	34.1756902757	51.7554617697
750	893.7644599995	1.0869486567	35.7964450415	54.5298878922
800	948.4066768769	1.0986858496	37.3699520751	57.2488200455
850	1003.6265321971	1.1100339660	38.9010908825	59.9181976996
900	1059.4019323282	1.1208949362	40.3940804368	62.5431553065
950	1115.7069194101	1.1312105169	41.8525925389	65.1281595279
1000	1172.5134122696	1.1409525145	43.2798419565	67.6771186900
1500	1762.1851200736	1.2100195314	56.3254722620	91.7815514376
2000	2377.1406412741	1.2462835672	68.0682900809	114.4862990907

Table A.1.1: Vectors of gas properties for semi perfect gas

A.2   Real gas tables

T [K]											
270	280	290	300	320	340	360	380	400	425	450	475

Table A.2.1: Temperature table of the real gas

p [bar]													
0.04	0.06	0.08	0.1	0.25	0.4	0.55	0.7	0.85	1	2	3	4	5

Table A.2.2: Pressure table of the real gas

$\rho \left[\frac{kg}{m^3}\right]$													
2.0572	3.1053	4.1672	5.2433	13.8337	13.8337	13.8337	13.8337	13.8337	13.8337	13.8337	13.8337	13.8337	13.8337
1.9807	2.9875	4.0058	5.0359	13.1846	13.1846	13.1846	13.1846	13.1846	13.1846	13.1846	13.1846	13.1846	13.1846
1.9100	2.8790	3.8576	4.8462	12.6095	21.1095	21.1095	21.1095	21.1095	21.1095	21.1095	21.1095	21.1095	21.1095
1.8443	2.7785	3.7208	4.6716	12.0940	20.1152	28.8950	38.6797	38.6797	38.6797	38.6797	38.6797	38.6797	38.6797
1.7261	2.5981	3.4761	4.3604	11.2019	18.4572	26.2018	34.5369	43.6044	53.6135	53.6135	53.6135	53.6135	53.6135
1.6225	2.4406	3.2632	4.0905	10.4509	17.1100	24.1069	31.4900	39.3201	47.6756	47.6756	47.6756	47.6756	47.6756
1.5309	2.3016	3.0758	3.8536	9.8055	15.9799	22.3982	29.0857	36.0721	43.3930	105.3519	105.3519	105.3519	105.3519
1.4492	2.1779	2.9094	3.6437	9.2424	15.0106	20.9607	27.1065	33.4636	40.0499	91.7150	168.6072	168.6072	168.6072
1.3759	2.0671	2.7606	3.4562	8.7452	14.1658	19.7251	25.4309	31.2918	37.3172	82.5919	140.8823	224.2950	224.2950
1.2942	1.9438	2.5950	3.2479	8.1986	13.2469	18.3965	23.6512	29.0152	34.4929	74.3021	121.3038	178.4978	250.1833
1.2217	1.8345	2.4485	3.0638	7.7196	12.4490	17.2537	22.1357	27.0970	32.1395	68.0018	108.3436	154.1413	206.4651
1.1570	1.7369	2.3179	2.8998	7.2957	11.7477	16.2566	20.8233	25.4485	30.1332	62.9524	98.7499	137.8501	180.5339

Table A.2.3: Density table of the real gas

$s \left[\frac{kJ}{K \cdot kg}\right]$													
1.7558	1.7251	1.7029	1.6855	1.6089	1.6089	1.6089	1.6089	1.6089	1.6089	1.6089	1.6089	1.6089	1.6089
1.7868	1.7562	1.7342	1.7169	1.6418	1.6418	1.6418	1.6418	1.6418	1.6418	1.6418	1.6418	1.6418	1.6418
1.8173	1.7869	1.7650	1.7479	1.6739	1.6317	1.6317	1.6317	1.6317	1.6317	1.6317	1.6317	1.6317	1.6317
1.8475	1.8172	1.7954	1.7784	1.7054	1.6643	1.6335	1.6073	1.6073	1.6073	1.6073	1.6073	1.6073	1.6073
1.9067	1.8766	1.8550	1.8381	1.7665	1.7272	1.6984	1.6748	1.6540	1.6347	1.6347	1.6347	1.6347	1.6347
1.9645	1.9345	1.9130	1.8963	1.8257	1.7874	1.7600	1.7379	1.7190	1.7020	1.7020	1.7020	1.7020	1.7020
2.0210	1.9911	1.9697	1.9530	1.8831	1.8457	1.8191	1.7980	1.7802	1.7645	1.7645	1.7645	1.7645	1.7645
2.0762	2.0463	2.0250	2.0084	1.9391	1.9022	1.8762	1.8558	1.8387	1.8238	1.7495	1.7495	1.7495	1.7495
2.1303	2.1004	2.0792	2.0626	1.9936	1.9571	1.9316	1.9117	1.8952	1.8808	1.8119	1.7591	1.7591	1.7591
2.1961	2.1664	2.1451	2.1286	2.0600	2.0239	1.9988	1.9794	1.9633	1.9495	1.8847	1.8388	1.7987	1.7599
2.2603	2.2305	2.2093	2.1929	2.1246	2.0887	2.0640	2.0448	2.0291	2.0156	1.9537	1.9116	1.8770	1.8457
2.3227	2.2930	2.2719	2.2554	2.1873	2.1517	2.1272	2.1083	2.0928	2.0795	2.0196	1.9801	1.9485	1.9212

Table A.2.4: Specific entropy table of the real gas

$h \left[\frac{kJ}{kg}\right]$													
367.0013	366.5662	366.1251	365.6777	362.0967	362.0967	362.0967	362.0967	362.0967	362.0967	362.0967	362.0967	362.0967	362.0967
375.5157	375.1241	374.7280	374.3271	371.1499	371.1499	371.1499	371.1499	371.1499	371.1499	371.1499	371.1499	371.1499	371.1499
384.2230	383.8687	383.5108	383.1491	380.3065	377.1895	377.1895	377.1895	377.1895	377.1895	377.1895	377.1895	377.1895	377.1895
393.1204	392.7980	392.4728	392.1446	389.5821	386.8121	383.7795	380.3986	380.3986	380.3986	380.3986	380.3986	380.3986	380.3986
411.4735	411.2023	410.9293	410.6545	408.5302	406.2820	403.8877	401.3171	398.5276	395.4558	395.4558	395.4558	395.4558	395.4558
430.5488	430.3164	430.0828	429.8480	428.0463	426.1670	424.2002	422.1340	419.9533	417.6388	417.6388	417.6388	417.6388	417.6388
450.3178	450.1154	449.9123	449.7083	448.1514	446.5439	444.8812	443.1580	441.3680	439.5038	424.2451	424.2451	424.2451	424.2451
470.7505	470.5720	470.3929	470.2132	468.8473	467.4476	466.0118	464.5374	463.0215	461.4610	449.5871	449.5871	449.5871	449.5871
491.8162	491.6569	491.4972	491.3371	490.1241	488.8880	487.6279	486.3425	485.0303	483.6901	473.9024	462.0608	462.0608	462.0608
518.9910	518.8512	518.7111	518.5708	517.5106	516.4360	515.3468	514.2423	513.1220	511.9854	503.9448	494.9359	484.6789	472.9262
547.0467	546.9226	546.7984	546.6740	545.7361	544.7894	543.8338	542.8691	541.8950	540.9113	534.0944	526.7795	518.9058	510.4543
575.9254	575.8143	575.7031	575.5919	574.7545	573.9119	573.0640	572.2108	571.3522	570.4882	564.5852	558.4241	551.9989	545.3273

Table A.2.5: Specific enthalpy table of the real gas

c_p $\left[\frac{kJ}{kg \cdot K}\right]$													
0.8417	0.8464	0.8513	0.8563	0.9008	0.9008	0.9008	0.9008	0.9008	0.9008	0.9008	0.9008	0.9008	0.9008
0.8611	0.8652	0.8693	0.8736	0.9102	0.9102	0.9102	0.9102	0.9102	0.9102	0.9102	0.9102	0.9102	0.9102
0.8803	0.8837	0.8873	0.8909	0.9214	0.9598	0.9598	0.9598	0.9598	0.9598	0.9598	0.9598	0.9598	0.9598
0.8992	0.9021	0.9051	0.9082	0.9339	0.9652	1.0047	1.0047	1.0047	1.0047	1.0047	1.0047	1.0047	1.0047
0.9359	0.9382	0.9404	0.9427	0.9613	0.9830	1.0087	1.0398	1.0398	1.0398	1.0398	1.0398	1.0398	1.0398
0.9714	0.9730	0.9748	0.9765	0.9904	1.0061	1.0239	1.0443	1.0681	1.0962	1.0962	1.0962	1.0962	1.0962
1.0053	1.0066	1.0080	1.0093	1.0201	1.0319	1.0448	1.0593	1.0754	1.0935	1.0935	1.0935	1.0935	1.0935
1.0377	1.0388	1.0399	1.0409	1.0494	1.0586	1.0685	1.0792	1.0909	1.1037	1.2318	1.2318	1.2318	1.2318
1.0686	1.0695	1.0703	1.0712	1.0781	1.0854	1.0932	1.1015	1.1104	1.1199	1.2052	1.3591	1.3591	1.3591
1.1050	1.1057	1.1064	1.1071	1.1125	1.1182	1.1242	1.1305	1.1372	1.1442	1.2016	1.2859	1.4138	1.4138
1.1391	1.1396	1.1402	1.1408	1.1452	1.1498	1.1545	1.1595	1.1647	1.1700	1.2118	1.2665	1.3382	1.4300
1.1709	1.1713	1.1718	1.1723	1.1760	1.1797	1.1836	1.1877	1.1918	1.1961	1.2281	1.2671	1.3142	1.3697

Table A.2.6: Specific heat at constant pressure table of the real gas

$\mu\,[s*uPa]$													
11.1760	11.1768	11.1779	11.1793	11.2032	11.2032	11.2032	11.2032	11.2032	11.2032	11.2032	11.2032	11.2032	11.2032
11.5993	11.6000	11.6009	11.6022	11.6222	11.6222	11.6222	11.6222	11.6222	11.6222	11.6222	11.6222	11.6222	11.6222
12.0212	12.0218	12.0226	12.0237	12.0407	12.0769	12.0769	12.0769	12.0769	12.0769	12.0769	12.0769	12.0769	12.0769
12.4415	12.4420	12.4427	12.4436	12.4582	12.4886	12.5399	12.5399	12.5399	12.5399	12.5399	12.5399	12.5399	12.5399
13.2759	13.2763	13.2768	13.2775	13.2885	13.3109	13.3472	13.4006	13.4006	13.4006	13.4006	13.4006	13.4006	13.4006
14.1007	14.1010	14.1014	14.1020	14.1106	14.1279	14.1551	14.1940	14.2468	14.3165	14.3165	14.3165	14.3165	14.3165
14.9145	14.9148	14.9151	14.9156	14.9226	14.9364	14.9578	14.9878	15.0276	15.0787	15.9012	15.9012	15.9012	15.9012
15.7165	15.7168	15.7171	15.7174	15.7233	15.7347	15.7522	15.7763	15.8078	15.8475	16.4114	16.4114	16.4114	16.4114
16.5061	16.5062	16.5065	16.5068	16.5118	16.5215	16.5361	16.5562	16.5821	16.6143	17.0404	18.0740	18.0740	18.0740
17.4749	17.4751	17.4753	17.4756	17.4798	17.4878	17.5000	17.5164	17.5375	17.5634	17.8876	18.5805	19.8864	22.2662
18.4236	18.4237	18.4239	18.4241	18.4278	18.4347	18.4450	18.4589	18.4766	18.4982	18.7587	19.2770	20.1598	21.5635
19.3523	19.3524	19.3526	19.3528	19.3560	19.3620	19.3710	19.3830	19.3982	19.4167	19.6340	20.0467	20.7103	21.6951

Table A.2.7: Dynamic viscosity table of the real gas

$k\,\left[\frac{mW}{K \cdot m}\right]$													
11.5202	11.5047	11.4895	11.4748	11.3824	11.3824	11.3824	11.3824	11.3824	11.3824	11.3824	11.3824	11.3824	11.3824
12.3521	12.3393	12.3268	12.3147	12.2386	12.2386	12.2386	12.2386	12.2386	12.2386	12.2386	12.2386	12.2386	12.2386
13.1848	13.1746	13.1646	13.1549	13.0948	13.0642	13.0642	13.0642	13.0642	13.0642	13.0642	13.0642	13.0642	13.0642
14.0186	14.0106	14.0030	13.9957	13.9509	13.9299	13.9443	14.0138	13.9443	13.9443	13.9443	13.9443	13.9443	13.9443
15.6889	15.6853	15.6819	15.6787	15.6627	15.6631	15.6852	15.7364	15.8283	15.7364	15.7364	15.7364	15.7364	15.7364
17.3633	17.3635	17.3638	17.3644	17.3743	17.3962	17.4327	17.4870	17.5639	17.6696	17.6696	17.6696	17.6696	17.6696
19.0419	19.0455	19.0492	19.0531	19.0864	19.1286	19.1811	19.2455	19.3240	19.4192	20.8756	20.8756	20.8756	20.8756
20.7249	20.7315	20.7382	20.7451	20.7996	20.8607	20.9291	21.0057	21.0916	21.1882	22.2508	22.2508	22.2508	22.2508
22.4123	22.4217	22.4311	22.4406	22.5144	22.5929	22.6765	22.7658	22.8614	22.9640	23.8923	25.5771	25.5771	25.5771
24.5281	24.5405	24.5530	24.5655	24.6609	24.7591	24.8606	24.9654	25.0740	25.1867	26.0690	27.2937	29.0982	31.7788
26.6511	26.6663	26.6814	26.6966	26.8113	26.9275	27.0453	27.1649	27.2865	27.4101	28.3006	29.3539	30.6544	32.2967
28.7815	28.7991	28.8167	28.8343	28.9663	29.0988	29.2317	29.3651	29.4990	29.6337	30.5551	31.5406	32.6283	33.8596

Table A.2.8: Thermal conductivity table of the real gas

$K_T[MPa]$													
0.0395	0.0589	0.0780	0.0968	0.2278	0.2278	0.2278	0.2278	0.2278	0.2278	0.2278	0.2278	0.2278	0.2278
0.0396	0.0590	0.0782	0.0972	0.2310	0.2310	0.2310	0.2310	0.2310	0.2310	0.2310	0.2310	0.2310	0.2310
0.0396	0.0591	0.0784	0.0975	0.2335	0.3542	0.3542	0.3542	0.3542	0.3542	0.3542	0.3542	0.3542	0.3542
0.0397	0.0592	0.0786	0.0978	0.2356	0.3606	0.4695	0.5576	0.4695	0.4695	0.4695	0.4695	0.4695	0.4695
0.0397	0.0594	0.0789	0.0983	0.2388	0.3699	0.4900	0.5973	0.6888	0.5973	0.5973	0.5973	0.5973	0.5973
0.0398	0.0595	0.0791	0.0986	0.2410	0.3763	0.5036	0.6219	0.7301	0.8267	0.8267	0.8267	0.8267	0.8267
0.0398	0.0596	0.0793	0.0989	0.2427	0.3809	0.5131	0.6386	0.7571	0.8677	1.3244	1.3244	1.3244	1.3244
0.0398	0.0597	0.0794	0.0991	0.2440	0.3844	0.5201	0.6507	0.7760	0.8957	1.5164	1.5164	1.5164	1.5164
0.0399	0.0597	0.0795	0.0992	0.2450	0.3871	0.5254	0.6598	0.7900	0.9160	1.6325	2.0777	2.0777	2.0777
0.0399	0.0598	0.0796	0.0994	0.2460	0.3897	0.5305	0.6683	0.8030	0.9346	1.7273	2.3564	2.8041	3.1138
0.0399	0.0598	0.0797	0.0995	0.2468	0.3917	0.5344	0.6747	0.8127	0.9483	1.7915	2.5261	3.1527	3.6953
0.0399	0.0598	0.0797	0.0996	0.2474	0.3933	0.5374	0.6796	0.8201	0.9587	1.8377	2.6408	3.3741	4.0547

Table A.2.9: Isothermal bulk modulus table of the real gas

$\alpha \left[\frac{1}{K}\right]$													
0.00387	0.00396	0.00405	0.00414	0.00500	0.00500	0.00500	0.00500	0.00500	0.00500	0.00500	0.00500	0.00500	0.00500
0.00371	0.00378	0.00386	0.00393	0.00462	0.00462	0.00462	0.00462	0.00462	0.00462	0.00462	0.00462	0.00462	0.00462
0.00356	0.00363	0.00369	0.00375	0.00431	0.00504	0.00504	0.00504	0.00504	0.00504	0.00504	0.00504	0.00504	0.00504
0.00343	0.00348	0.00354	0.00359	0.00405	0.00463	0.00538	0.00642	0.00538	0.00538	0.00538	0.00538	0.00538	0.00538
0.00320	0.00324	0.00327	0.00331	0.00363	0.00402	0.00448	0.00505	0.00578	0.00505	0.00505	0.00505	0.00505	0.00505
0.00300	0.00302	0.00305	0.00308	0.00332	0.00359	0.00389	0.00425	0.00467	0.00517	0.00517	0.00517	0.00517	0.00517
0.00282	0.00284	0.00286	0.00289	0.00306	0.00326	0.00348	0.00372	0.00400	0.00431	0.00431	0.00431	0.00431	0.00431
0.00267	0.00268	0.00270	0.00272	0.00286	0.00300	0.00317	0.00334	0.00353	0.00374	0.00589	0.00589	0.00589	0.00589
0.00253	0.00254	0.00256	0.00257	0.00268	0.00279	0.00292	0.00305	0.00319	0.00334	0.00470	0.00717	0.00717	0.00717
0.00237	0.00238	0.00240	0.00241	0.00249	0.00258	0.00267	0.00277	0.00287	0.00297	0.00384	0.00509	0.00697	0.00971
0.00224	0.00225	0.00226	0.00226	0.00233	0.00240	0.00247	0.00254	0.00262	0.00269	0.00329	0.00405	0.00502	0.00622
0.00212	0.00213	0.00213	0.00214	0.00219	0.00224	0.00230	0.00236	0.00241	0.00247	0.00290	0.00341	0.00401	0.00468

Table A.2.10: isobaric thermal expansion coeffient table of the real gas

A.3   Performance maps

A.3.1   Perfect gas
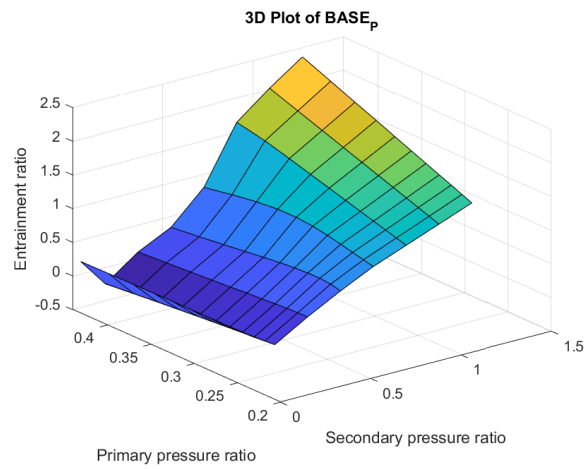
Figure A.3.1: Semi perfect gas base case

(a) 0.85

(b) 0.95
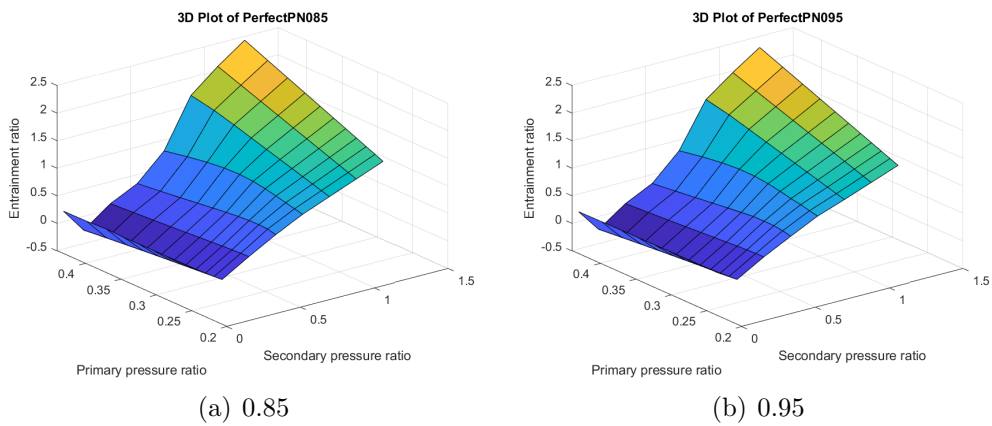
Figure A.3.2: Efficiency of the primary flow through the nozzle

(a) 0.8

(b) 0.9
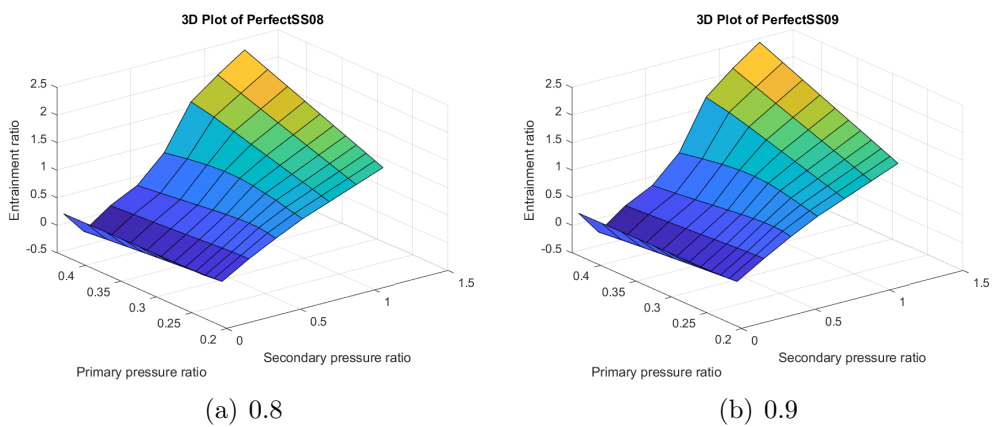
Figure A.3.3: Efficiency of the secondary flow suction

(a) 0.8   (b) 0.9
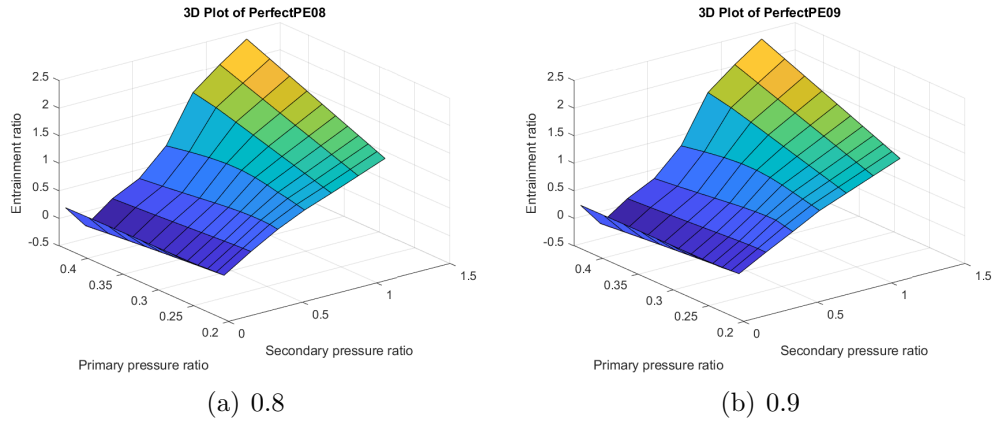
Figure A.3.4: Efficiency of the primary flow expansion

(a) 0.8   (b) 0.9
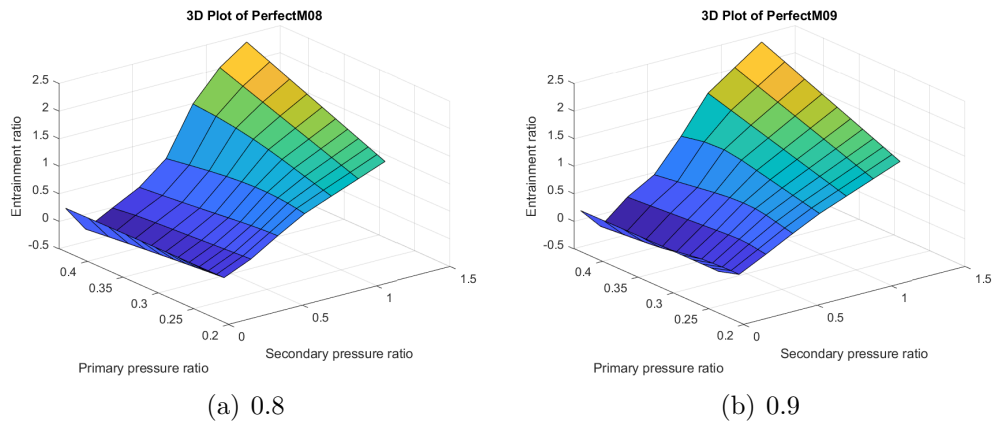
Figure A.3.5: Efficiency of the primary flow expansion

A.3.2   Semi-perfect gas
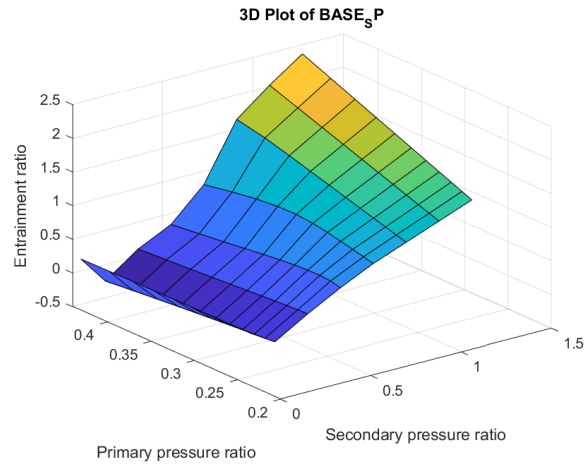
Figure A.3.6: Perfect gas base case

(a) 0.85   (b) 0.95
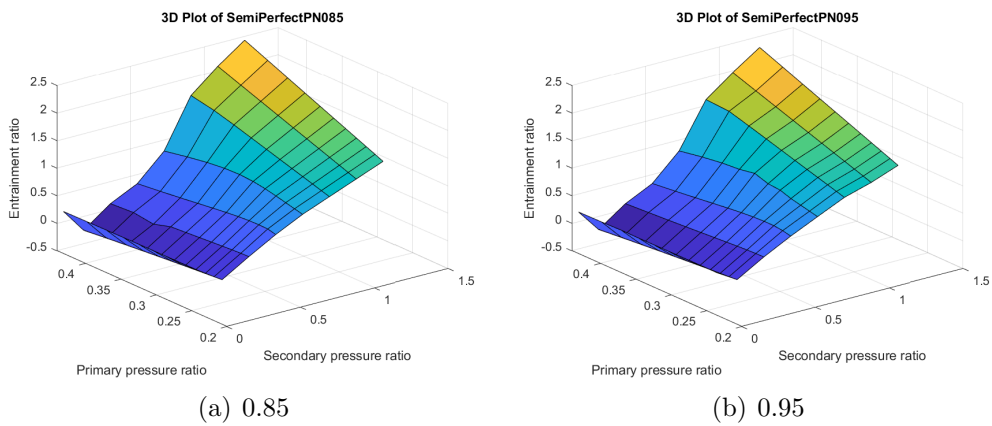
Figure A.3.7: Efficiency of the primary flow through the nozzle

(a) 0.8   (b) 0.9
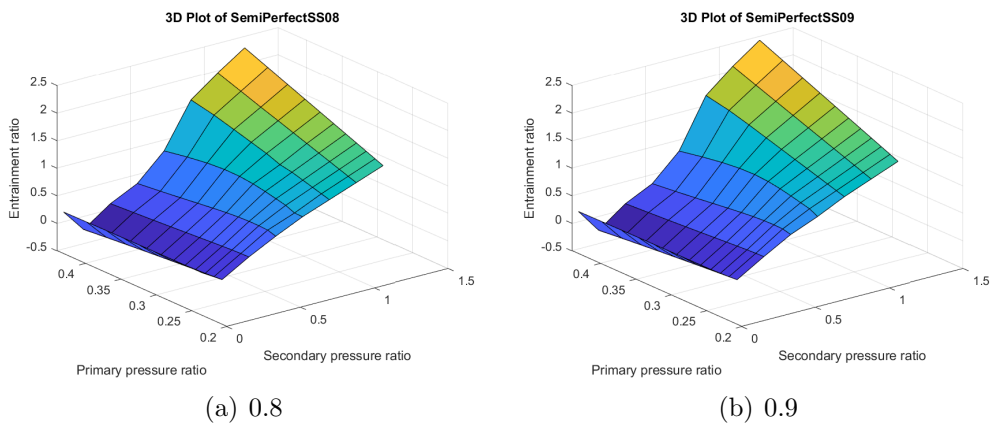
Figure A.3.8: Efficiency of the secondary flow suction

(a) 0.8

(b) 0.9
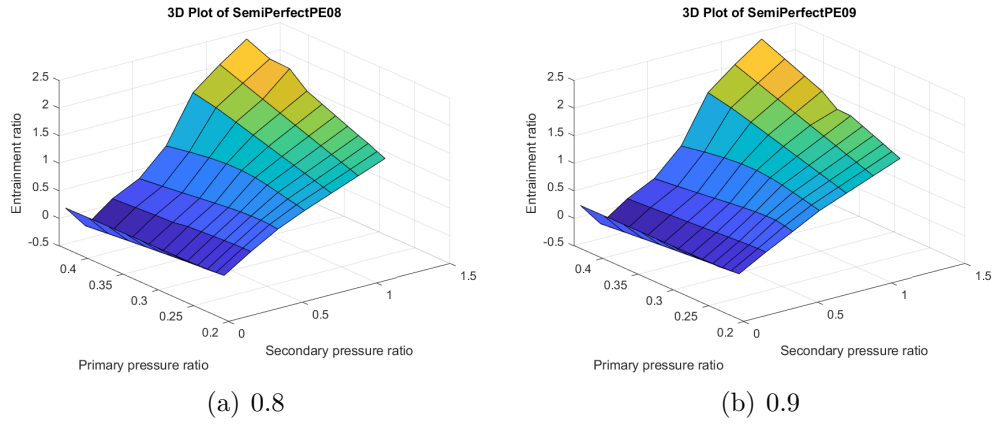
Figure A.3.9: Efficiency of the primary flow expansion

(a) 0.8

(b) 0.9
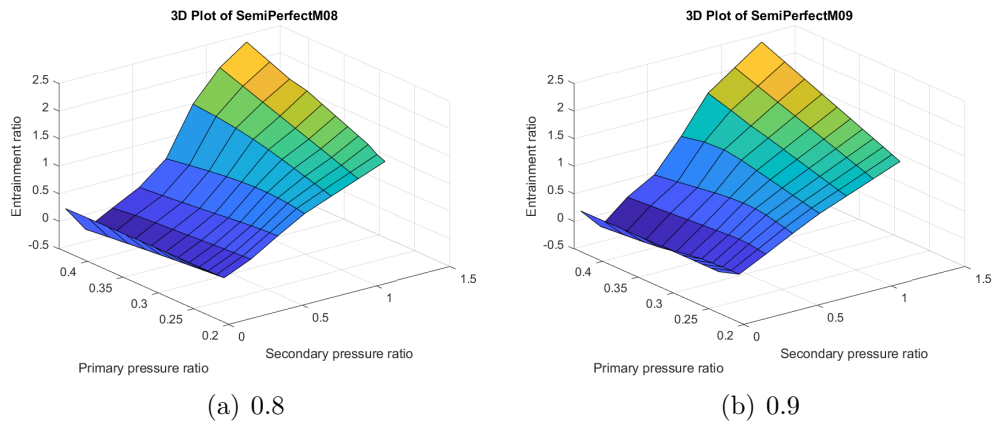
Figure A.3.10: Efficiency of the primary flow expansion

A.3.3   Real gas
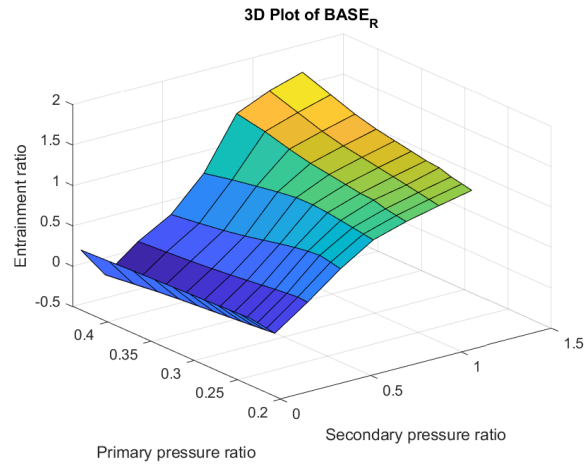
Figure A.3.11: Real gas base case

(a) 0.85   (b) 0.95
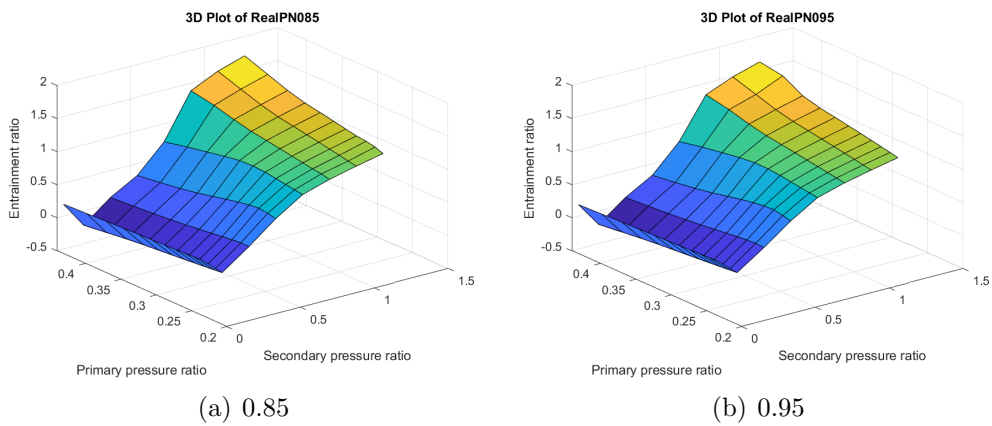
Figure A.3.12: Efficiency of the primary flow through the nozzle

(a) 0.8   (b) 0.9
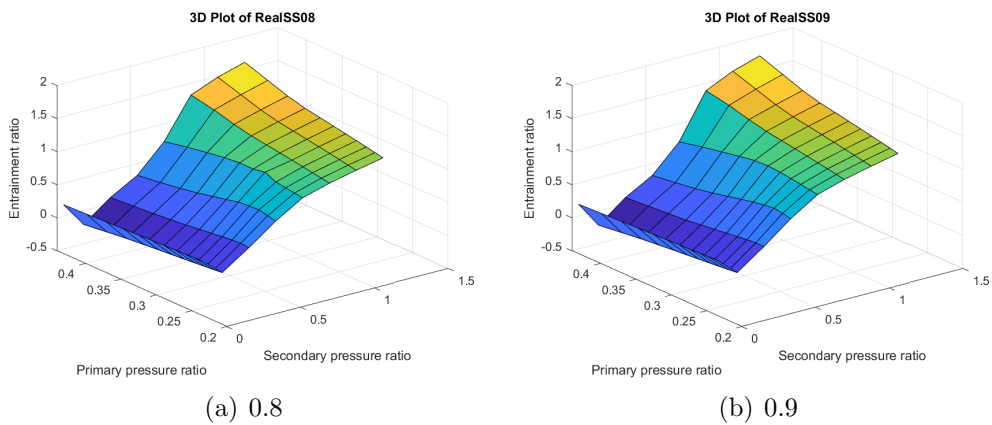
Figure A.3.13: Efficiency of the secondary flow suction

(a) 0.8   (b) 0.9
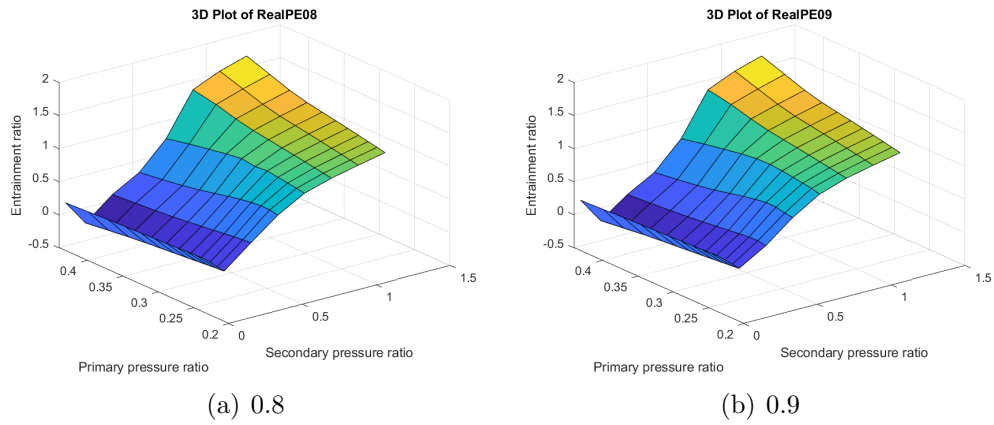
Figure A.3.14: Efficiency of the primary flow expansion

(a) 0.8   (b) 0.9
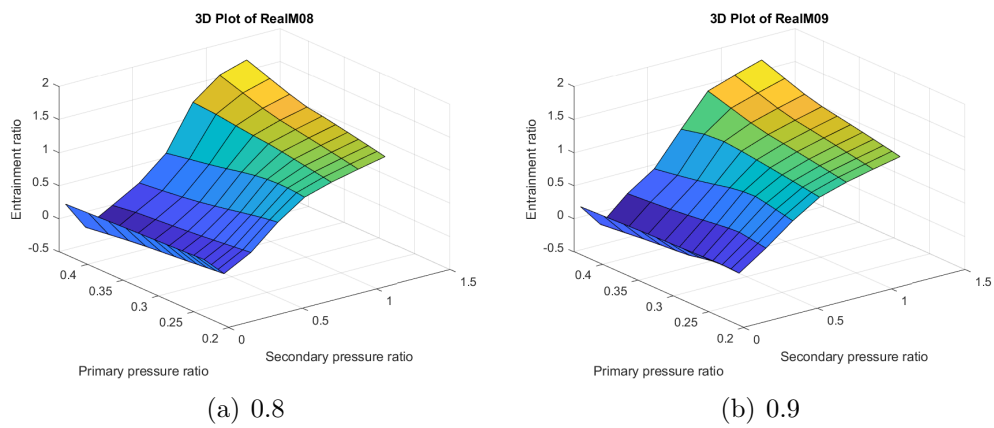
Figure A.3.15: Efficiency of the primary flow expansion

A.4   2D plots maps

A.4.1   Semi perfect gas

- Secondary flow suction efficiency

(a) $\Pi_{po} = 0.44$
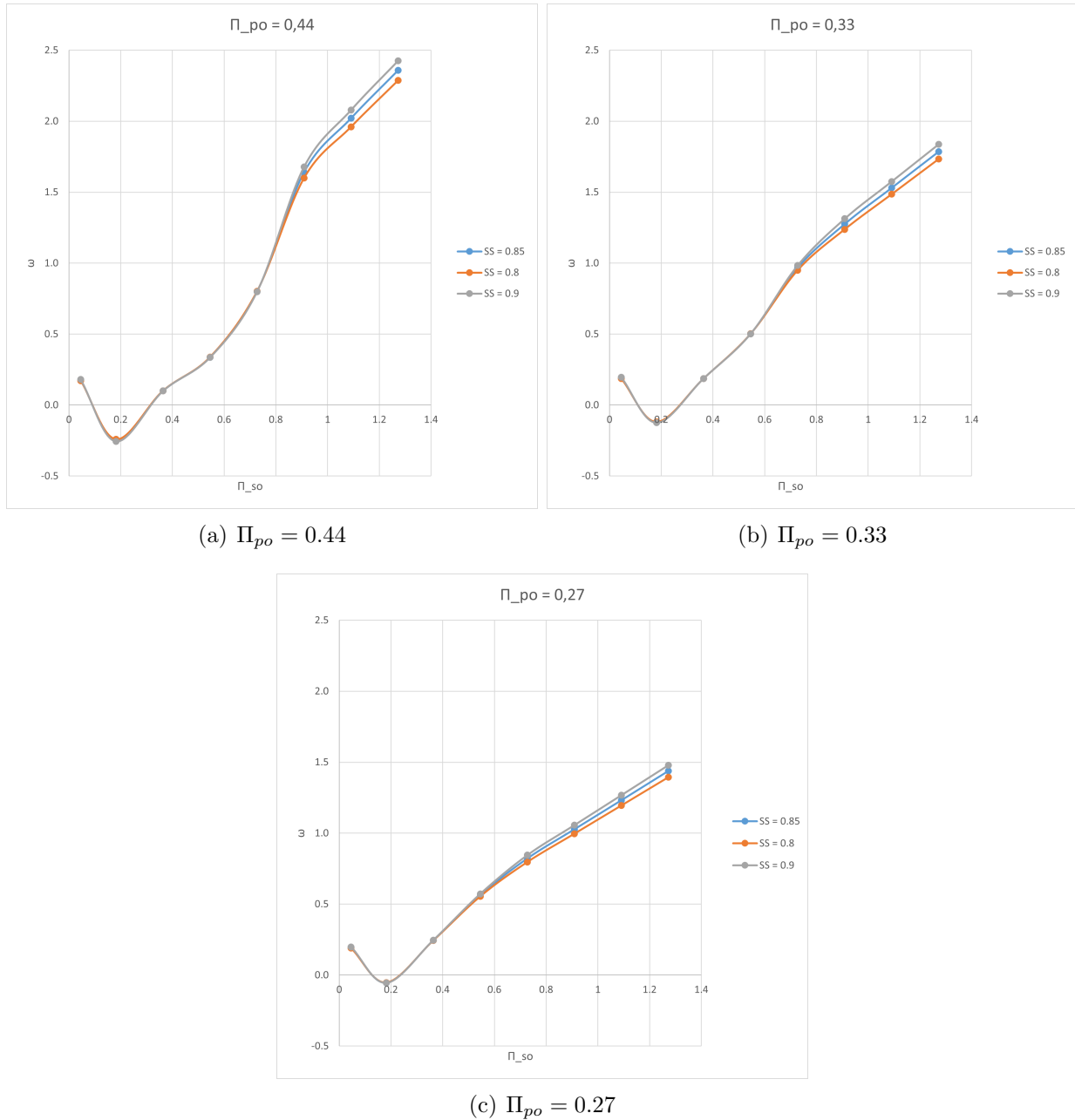
(b) $\Pi_{po} = 0.33$

(c) $\Pi_{po} = 0.27$

Figure A.4.1: Effect of η_{SS}

- Primary flow through nozzle efficiency
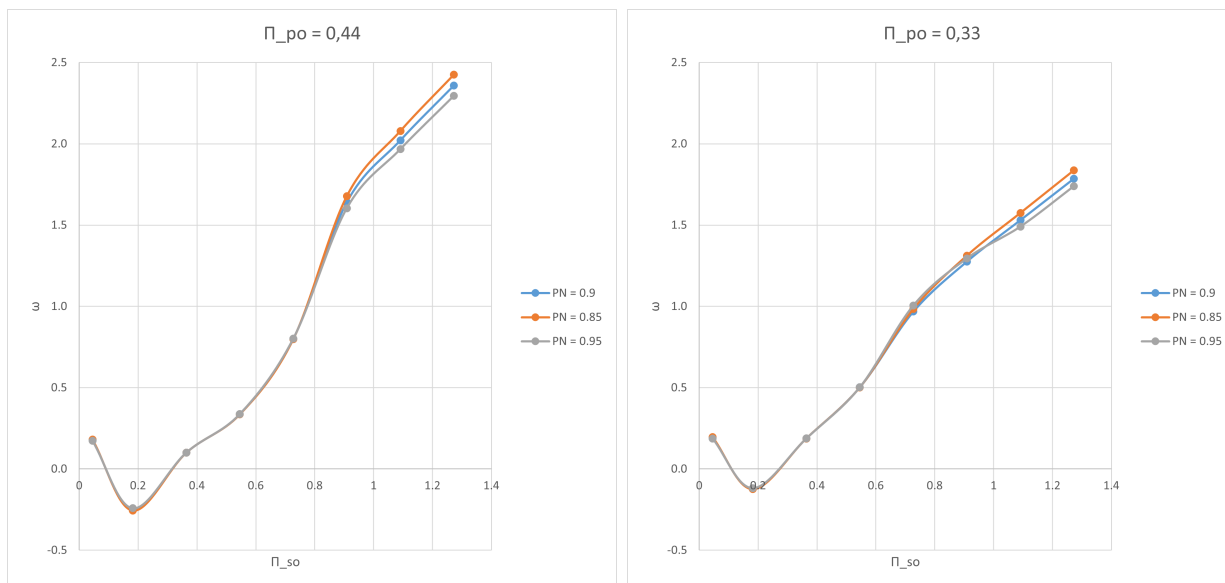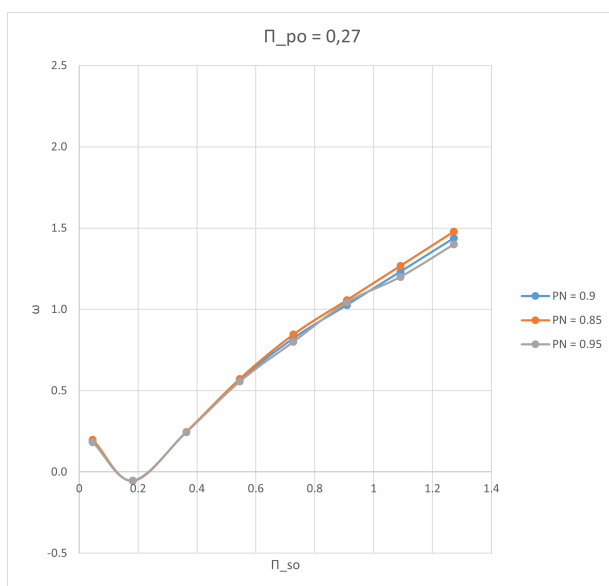
(a) $\Pi_{po} = 0.44$

(b) $\Pi_{po} = 0.33$

(c) $\Pi_{po} = 0.27$

Figure A.4.2: Effect of η_{PN}

- Primary flow expansion efficiency
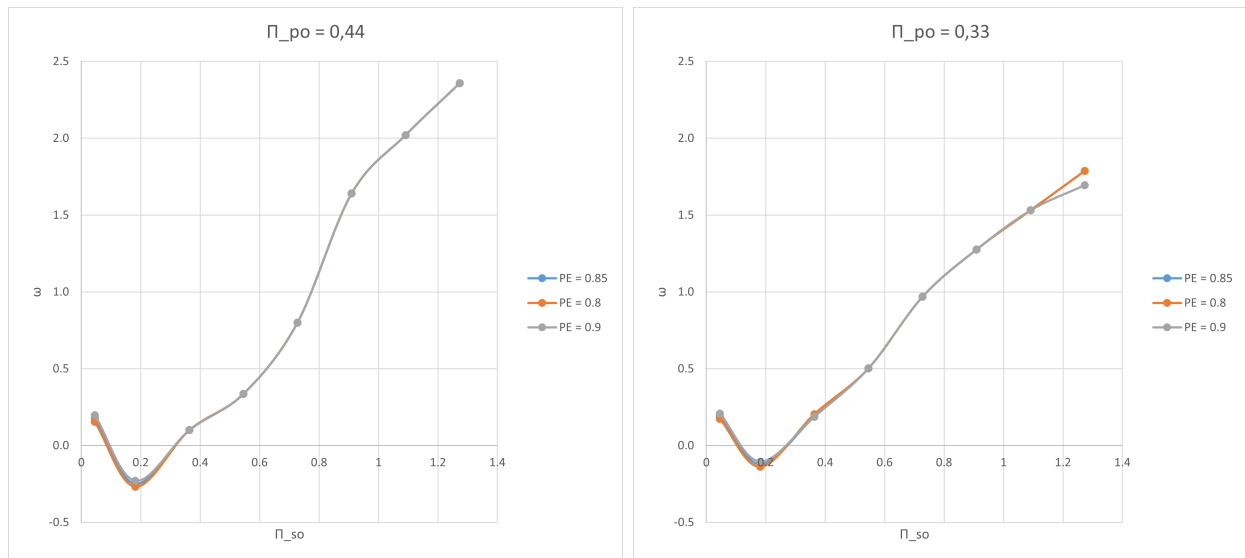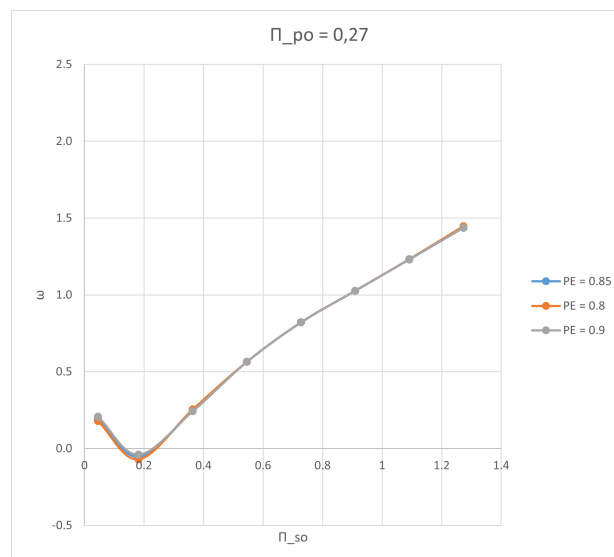
(a) $\Pi_{po} = 0.44$

(b) $\Pi_{po} = 0.33$

(c) $\Pi_{po} = 0.27$

Figure A.4.3: Effect of η_{PE}

- Mixing efficiency
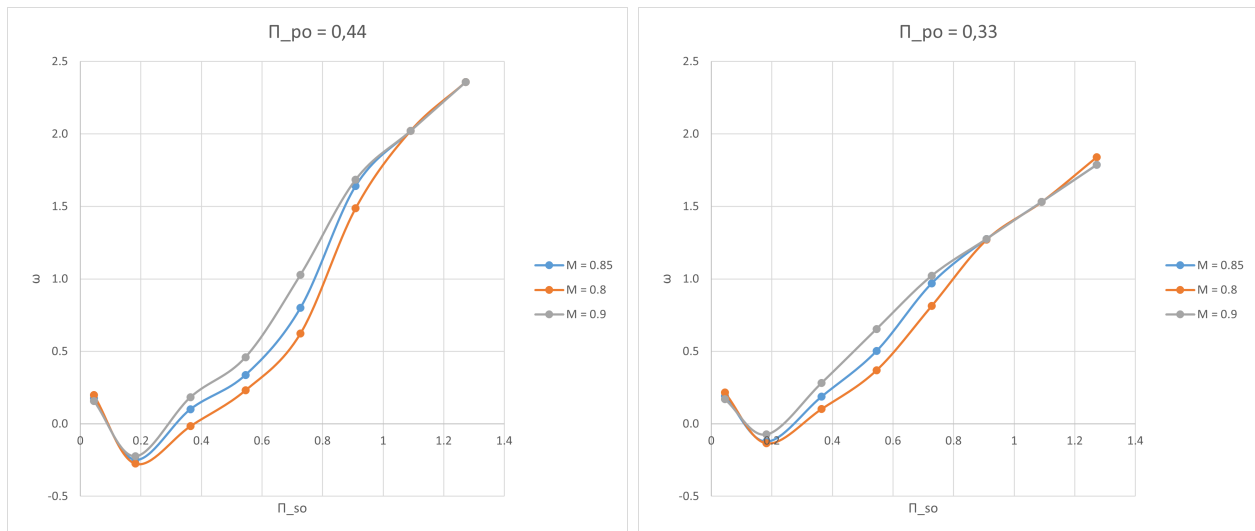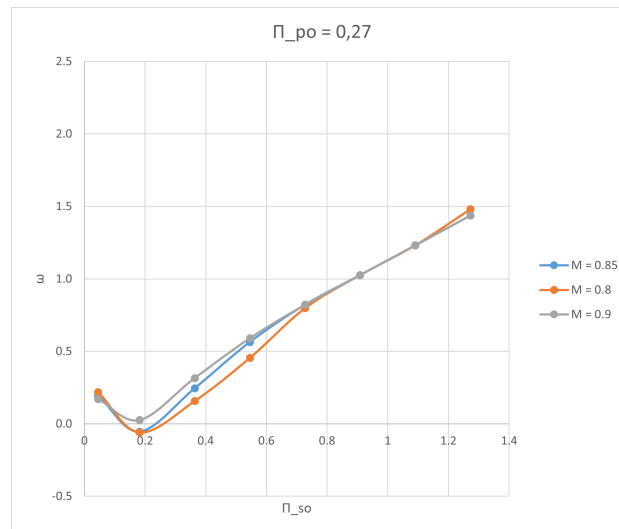
(a) $\Pi_{po} = 0.44$

(b) $\Pi_{po} = 0.33$

(c) $\Pi_{po} = 0.27$

Figure A.4.4: Effect of η_M

A.4.2   Real gas

- Secondary flow suction efficiency

(a) $\Pi_{po} = 0.44$
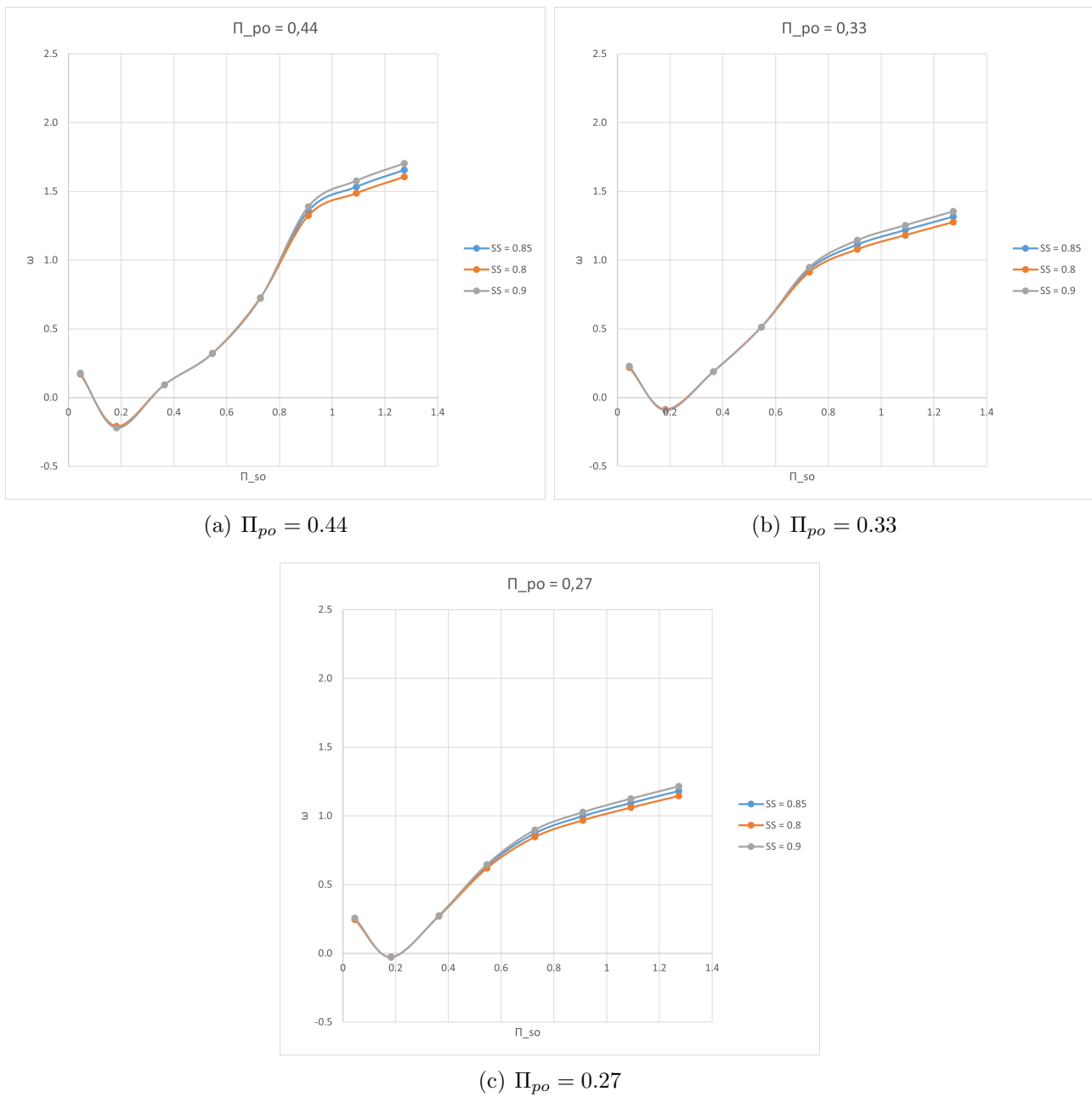
(b) $\Pi_{po} = 0.33$

(c) $\Pi_{po} = 0.27$

Figure A.4.5: Effect of η_{SS}

- Primary flow through nozzle efficiency
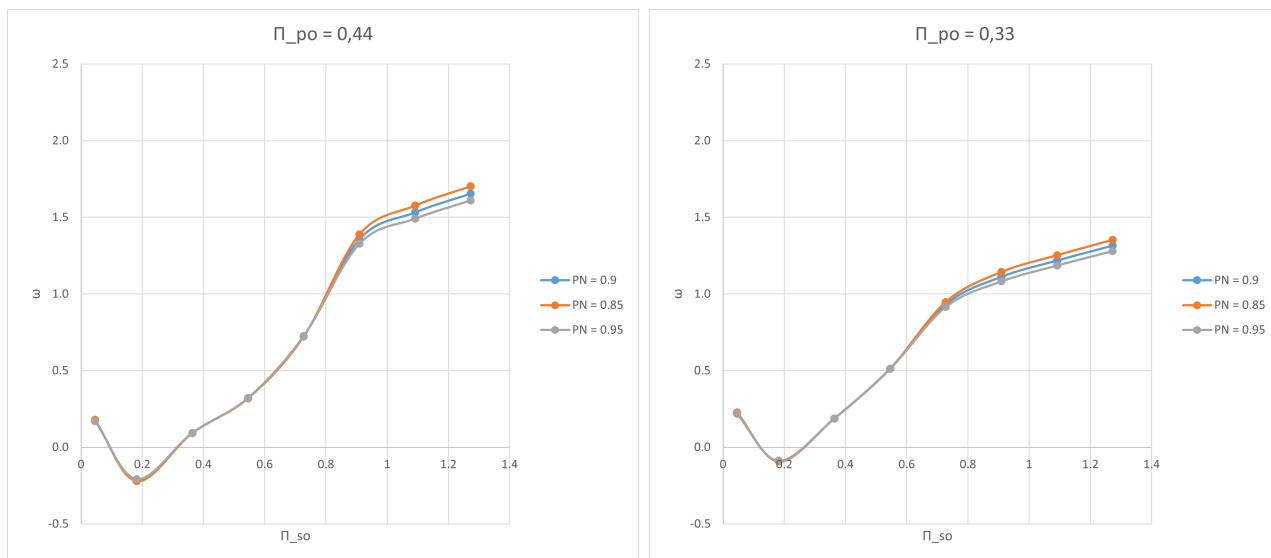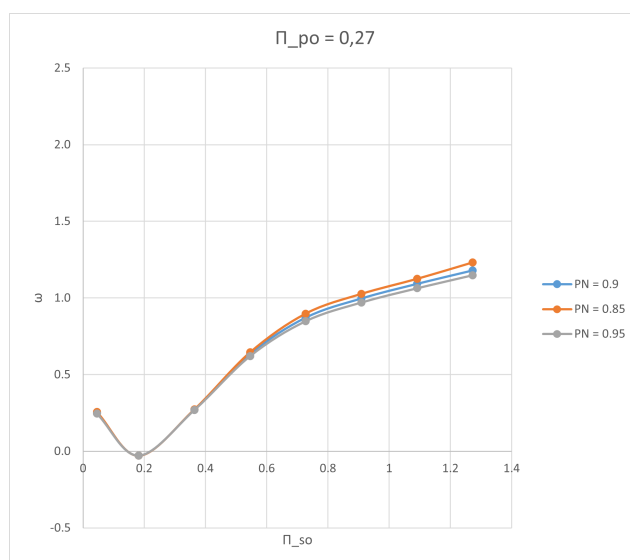
(a) $\Pi_{po} = 0.44$

(b) $\Pi_{po} = 0.33$

(c) $\Pi_{po} = 0.27$

Figure A.4.6: Effect of η_{PN}

• Primary flow expansion efficiency
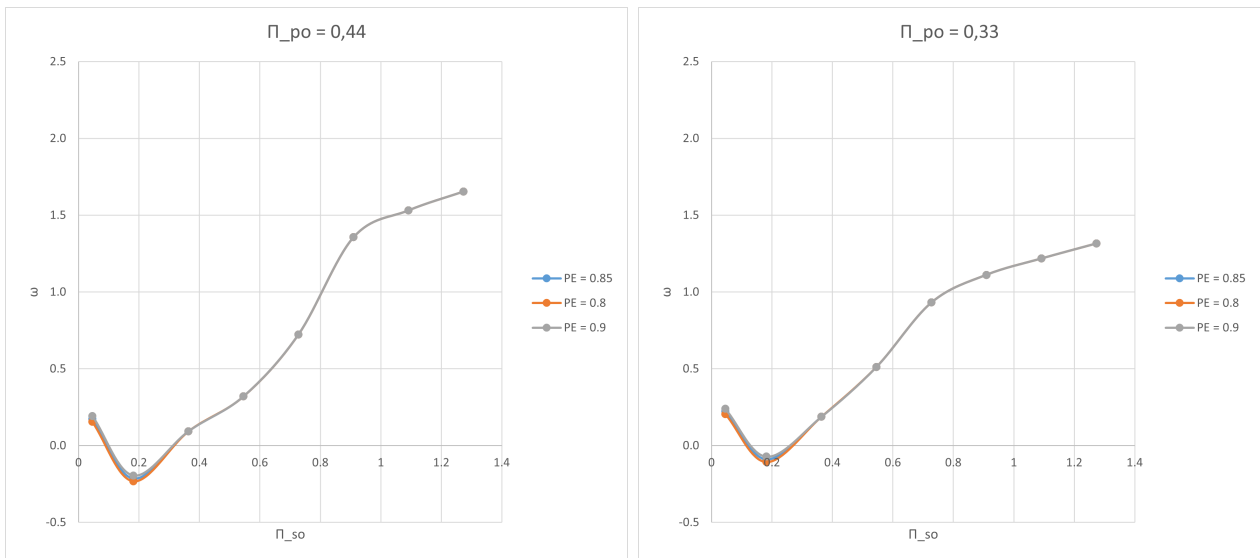
(a) $\Pi_{po} = 0.44$

(b) $\Pi_{po} = 0.33$
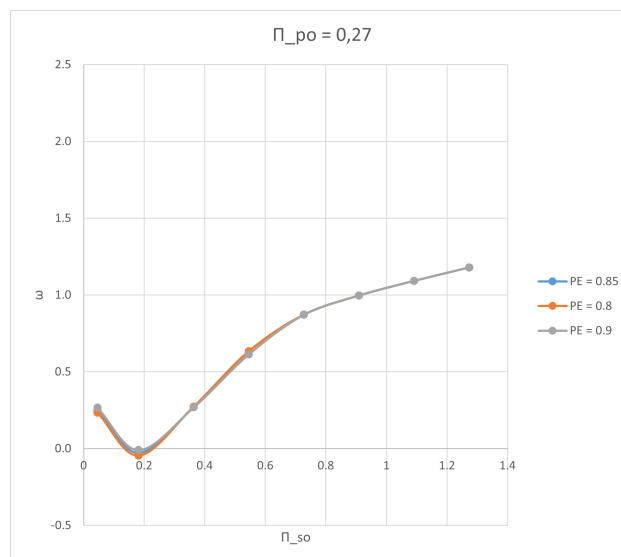
(c) $\Pi_{po} = 0.27$

Figure A.4.7: Effect of η_{PE}

• Mixing efficiency

(a) $\Pi_{po} = 0.44$

(b) $\Pi_{po} = 0.33$

(c) $\Pi_{po} = 0.27$
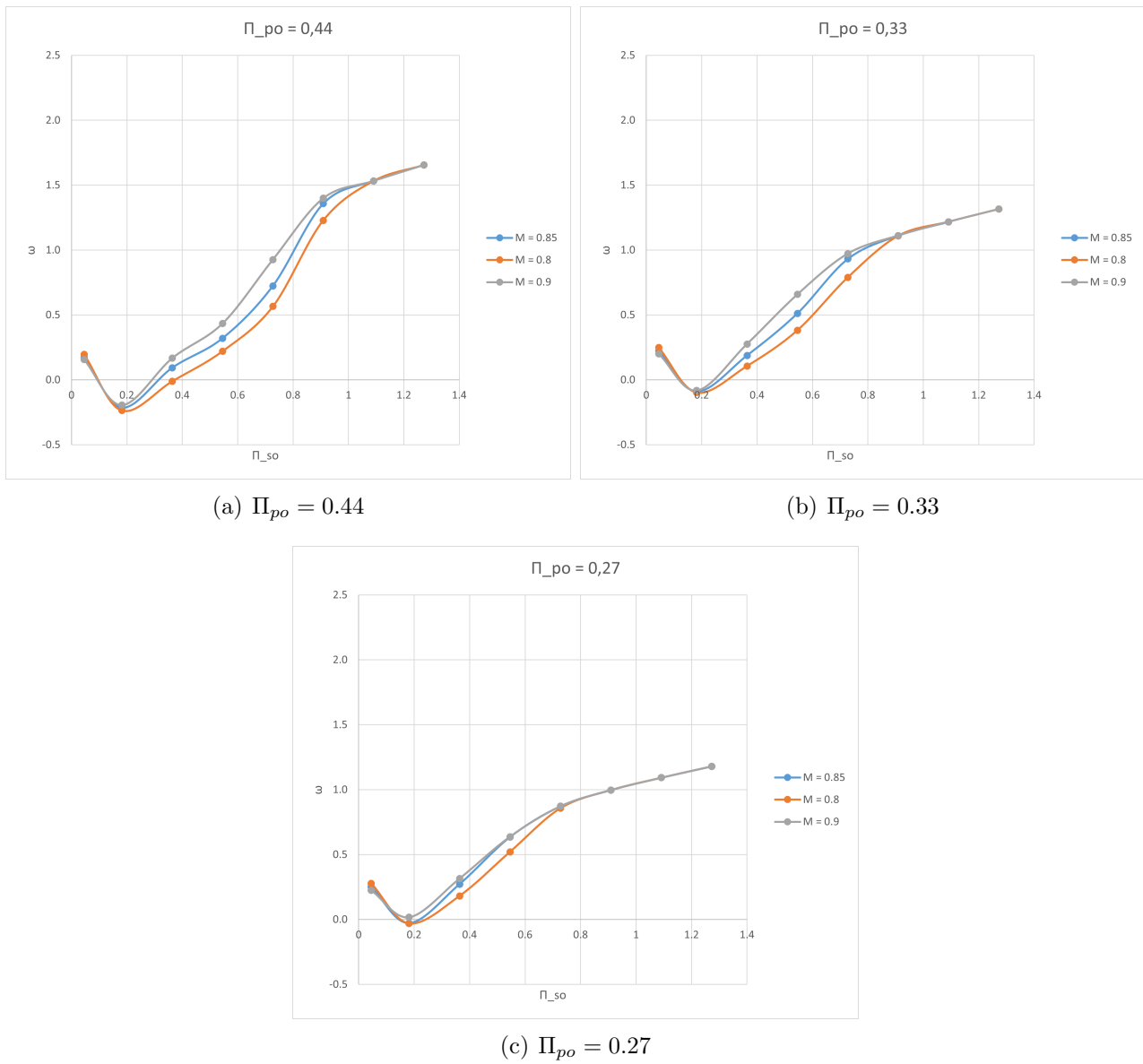
Figure A.4.8: Effect of η_M

A.5   Scopes statement

The scope statement details the project deliverables and describes the major objectives. Considering this project has a theoretical nature, the scope statements will focus on the setting of the conditions of the working environment.

This final degree project has a main objective the application of all the knowledge acquired throughout the academic years in the resolution of a real life problem. Bearing this in mind, the choice of the topic at study was performed considering the fact that it opened doors to explore a very common phenomena, which is thermal systems, in an application environment that was not the primary focus of the degree studied.

With the aim of performing any project, the worker requires of certain environmental characteristics that will not only ease the process by reducing distractions and thus increasing efficiency, but also will consider its health and well being so that it can continue to contribute to the research or maintenance which he is in charge of. These can be categorised as the working environment conditions.

On the other hand, proper, efficient, precise and reliable equipment ensures not only fast and accurate results, but also increases the efficiency of the worker. All the characteristics and requirements of the equipment needed to perform the task at hand are detailed in the section of working equipment conditions.

A.5.1   Working environment conditions

Seeing that this project has been developed in Spain, and that it is fully a digital project, implying the continuous and long exposure to screens, the decree that is in charge of the regulations of the workplace is the *Real Decreto 488/1997 del 14 de Abril* [2], which regulates all the tasks that require equipment with visualization screens.

The variables that asses the risks that a worker is exposing themselves to are:

- Time spent working in front of the screen.

- Attention time required in front of the screen.

- Degree of complexity of the task at hand.

- Need for rapid information acquisition.

These can entail different risks:

- Electrical circuit hazard
  The electrical circuit should be installed and maintained by an authorised company.

- Industrial hygiene:

- Illumination:

  General illumination should have enough level, as well as having the proper relationship with respect to the screen illumination according to the user needs.

  Illumination should be in a way that avoid flashes.

- Noise:

  The noise produced by the equipment should be taken into account when designing the same, so that they do not cause discomfort or disturb communication.

- Heat:

  The equipment employed should not generate additional heat that could entail discomfort for the workers.

- Humidity:

  Should have comfortable levels.

- Ergonomics

  - Desk:

    Should have enough dimension to allow the placement of the equipment, as well as all the required additional documentation. Should be balanced so as to ensure comfort.

  - Seat: Should be stable, ensuring additionally freedom of movement and guaranteeing a proper posture.

    Should have adjustable height and regulated backrest so as to be regulated for diverse users.

- Visual, physical and mental fatigue.

  - Screen:

    The characters should be well defined and configured, with a sufficient dimension as well as enough spacing between characters and lines.

    The image should be clear, without flashes or any other instabilities.

    The screen settings should be easily accessible to increase comfort, as well as being able to be turned and disposed in the optimal position to the user.

  - Keyboard:

    It should be separated from the screen, enabling proper posture and comfort. There should be enough space for the worker to rest their forearms.

    The keyboard should have a keys disposition that facilitates its usage, as well as matte surface to avoid flashes.

A.5.2   Working equipment conditions

For the achievement of the calculations required for the work, informatics resources, which are divided in hardware and software, are required.

- Hardware

  It is an HP computer with an processor Intel(R) Core(TM) i7-1065G7 CPU @ 1.30GHz. An installed ram of 16 GM (with 15.7 GB usable)

- Software

  This project is mainly based on the utilisation of the Matlab software, more specifically on the Simscape library, for the simulation of the cases and the obtainment of the numerical results required. The prostprocessing was done not only using Matlab software, but also Excel, from the Microsoft Office 365 package.

List of Figures

List of Tables

References

[1] Graham Engineering Answers. Ejectors. www.graham-mfg.com.

[2] Boletín Oficial del Estado (Official State Buletin) BOE. Real decreto 488/1997, de 14 de abril, sobre disposiciones mínimas de seguridad y salud relativas al trabajo con equipos que incluyen pantallas de visualización. 1997.

[3] Super Radiator Coils. The 4 main refrigeration cycle components. www.superradiatorcoils.com.

[4] HVAC engineering. Refrigerant ph chart. www.hvac-eng.com.

[5] Vicente Dolz Alberto Ponce-Mora José Galindo, Antonio Gil. Numerical optimization of an ejector for waste heat recovery used to cool down the intake air in an internal combustion engine. October 2020.

[6] Johannes Uhlig Klaus Buchne. Discussion on energy saving and emission reduction technology of heat treatment equipment. March 2023.

[7] mathWorks. Ejector (g). www.mathworks.com.

[8] mathWorks. Gas models. www.mathworks.com.

[9] United Nations. Sustainable development goals. www.undp.org.

[10] Skill and Lync. Hemant dagade. www.skill-lync.com.

[11] transvac. Principle of operation of ejectors. www.transvac.co.uk.

[12] Zhenying Zhang. Energetic and exergetic analysis of an ejector-expansion refrigeration cycle using the working fluid r32. *The Computer Journal*, 2015.

[13] X. Zheng and T.S. Ge. 14 - other types of solar-powered cooling systems. In R.Z. Wang and T.S. Ge, editors, *Advances in Solar Heating and Cooling*, pages 381–396. Woodhead Publishing, 2016.